

Heat-producing elements in the lunar mantle: Insights from ion microprobe analyses of lunar pyroclastic glasses

Justin J. Hagerty ^{a,*}, Charles K. Shearer ^a, David T. Vaniman ^b

^a Institute of Meteoritics, Department of Earth and Planetary Sciences, University of New Mexico, MSC03-2050, Albuquerque, NM 87131-0001, USA

^b Los Alamos National Laboratory, Hydrology, Geochemistry, and Geology, MS D462, Los Alamos, NM 87545, USA

Received 17 November 2005; accepted in revised form 19 April 2006

Abstract

We provide new estimates for the abundance of heat-producing elements in the lunar mantle by using SIMS techniques to measure the concentrations of thorium and samarium in lunar pyroclastic glasses. Lunar pyroclastic glasses are utilized in this study because they represent quenched products of near-primary melts from the lunar mantle and as such, they provide compositional information about the mantle itself. Thorium and samarium were measured because: (1) Th is not significantly fractionated from Sm during partial melting of the pyroclastic glass source regions, which are dominated by olivine and pyroxene. Therefore, the Th/Sm ratios that we measure in the pyroclastic glasses reflect the Th/Sm ratio of the pyroclastic glass source regions. (2) Strong correlations between Th, U, and K on the Moon allow us to use measured Th concentrations to estimate the concentrations of U and K in the pyroclastic glasses. (3) Th, Sm, U, and K are radioactive elements and as such, their concentrations can be used to investigate heat production in the lunar mantle.

The results from this study show that the lunar mantle is heterogeneous with respect to heat-producing elements and that there is evidence for mixing of a KREEP component into the source regions of some of the pyroclastic glasses. Because the source regions for many of the glasses are deep (≥ 400 km), we propose that a KREEP component was transported to the deep lunar mantle. KREEP enriched sources produce 138% more heat than sources that do not contain KREEP and therefore, could have provided a source of heat for extended periods of nearside basaltic magmatism. Data from this study, in conjunction with models for the fractional crystallization of a lunar magma ocean, are used to show that the average lunar mantle contains 0.15 ppm Th, 0.54 ppm Sm, 0.039 ppm U, and 212 ppm K. This is a greater enrichment in radiogenic elements than some earlier estimates, suggesting a more prolonged impact of radiogenic heat on nearside basaltic volcanism.

© 2006 Elsevier Inc. All rights reserved.

1. Introduction

The global asymmetry of thorium on the lunar surface (e.g., Haskin, 1997; Haskin et al., 2000; Lawrence et al., 1998, 2000, 2003) correlates well with the distribution of mare basalts, indicating that there is a significant linkage between the heat-producing elements and the thermal and magmatic evolution of the Moon. A firmer understanding of this linkage can be obtained by determining the lunar inventory of heat-producing elements such as Th, U, and

K. Previous studies have estimated the abundance of heat-producing elements in the lunar crust (O'Neill, 1991; Taylor et al., 2002; Jolliff and Gillis, 2002; Warren and Humphrys, 2003; Warren, 2005) and for the bulk Moon (Anders, 1977; Wänke et al., 1977; Taylor, 1994); however, few studies have attempted to estimate the abundance and distribution of these elements in the lunar mantle.

Lunar pyroclastic glasses provide a means for understanding how heat-producing elements are distributed in the lunar mantle. First, lunar pyroclastic glasses represent quenched products of near-primary melts from the lunar mantle (Stolper et al., 1974; Green et al., 1975; Delano, 1980; Chen et al., 1982; Chen and Lindsley, 1983). Second, lunar pyroclastic glasses appear to represent melting of a diverse range of mantle mineral assemblages (Shearer and

* Corresponding author. Present address: Los Alamos National Laboratory, Space Science and Applications, MS D466, Los Alamos, NM 87545, USA. Fax: +1 505 665 7395.

E-mail address: jhagerty@lanl.gov (J.J. Hagerty).

Papike, 1993, 1999). Third, high-pressure experiments indicate that the lunar pyroclastic glasses represent basaltic melts that were in equilibrium with olivine + orthopyroxene residua (Stolper et al., 1974; Green et al., 1975; Delano, 1980; Chen et al., 1982; Chen and Lindsley, 1983; Longhi, 1992; Hess, 2000; Elkins-Tanton et al., 2003). This residual mineral assemblage does not significantly fractionate Th from Sm during melting, which means that the Th/Sm ratio of the glasses approximates the Th/Sm ratio of the mantle sources from which the melts were derived (Shearer et al., 2002). Finally, previous studies of the lunar sample suite have shown that there are strong correlations between Th and U as well as between Th and K (e.g., Korotev, 1998). Therefore, U and K concentrations can be estimated by measuring the concentration of Th.

Here, we use new ion microprobe data for Th and Sm in lunar pyroclastic glasses to calculate the abundance of heat-producing elements in individual mantle sources and in the bulk lunar mantle. These calculations enable a better estimate of the heat production within the lunar mantle and may therefore provide additional insight into the thermal and chemical evolution of the Moon as a whole.

2. Basaltic source regions in the lunar mantle

Previous studies have proposed that rapid, hot accretion of the Moon led to early global melting (i.e., lunar magma ocean) (Smith et al., 1970; Wood et al., 1970). Models for crystallization of a dynamically simple lunar magma ocean (LMO) indicate that as the LMO cooled, it underwent an approximate crystallization sequence: olivine → orthopyroxene + olivine → plagioclase + olivine + pigeonite → clinopyroxene + plagioclase + pigeonite → pigeonite + plagioclase + clinopyroxene + ilmenite (Taylor and Jäkes, 1974; Snyder et al., 1992; Shearer and Papike, 1999). The crystallization sequence described above would have concentrated incompatible trace-elements in the late-stage, evolved liquid of the LMO by exclusion from the crystal structures of olivine, pyroxene, and plagioclase (e.g., Warren and Wasson, 1979; Snyder et al., 1992). Petrologic models predict that this residual melt, referred to as urKREEP (ur = primeval), was enriched in K, REE, and P ("KREEP"), as well as Th, U, Zr, Hf, Nb, and other incompatible elements (Warren and Wasson, 1979).

The distribution of cumulates within the lunar mantle is commonly described with one of two models, both of which predict a variety source regions for lunar basalts. The first model predicts that the lunar mantle remains stratified and that heat-producing elements are located just beneath the lunar crust (Snyder et al., 1992). The LMO crystallization sequence of Snyder et al. (1992) also predicts a relationship between basalt compositions and depth of source. In other words, the model predicts that high-Ti basalt sources are shallow and low-Ti basalt sources are deep. Experimental studies, however, do not support such a relationship (e.g., Longhi, 1987, 1992). In fact, experimental studies suggest that high-Ti and low-Ti basalts come from

a variety of depths (Stolper et al., 1974; Green et al., 1975; Delano, 1980; Chen et al., 1982; Chen and Lindsley, 1983; Longhi, 1992; Elkins-Tanton et al., 2000, 2003). The variable depths of the high-Ti and low-Ti source regions can be explained by a second petrologic model that involves gravitational destabilization and subsequent overturn of LMO cumulates (e.g., Hughes et al., 1988; Shearer et al., 1991; Spera, 1992; Hess and Parmentier, 1995).

The gravity-induced overturn model is based on the assumption that LMO crystallization would have led to a progressive enrichment in FeO with crystallization, increasing the density of late-stage cumulates (Taylor and Jäkes, 1974; Snyder et al., 1992; Shearer and Papike, 1999). The increase in density would have created a gravitationally unstable mineral stratigraphy with dense, FeO-rich, phases overlying less dense, MgO-rich phases. Gravitational instability could have been alleviated by overturn of the cumulate pile (e.g., Shearer et al., 1990, 1991; Ryder, 1991; Spera, 1992; Shearer and Papike, 1993; Hess and Parmentier, 1995). Potentially, overturn of the cumulate pile would have transported evolved cumulates (including KREEP and heat-producing elements) to various depths in the lunar mantle, producing compositionally diverse source regions (Shearer and Papike, 1999). Transport and subsequent decay of radioactive elements at various depths in the lunar mantle provided heat for melting LMO cumulates (Shearer and Papike, 1999), with resulting melts being erupted in the form of mare basalts and pyroclastic glasses (Shearer and Papike, 1993). Dynamical modeling of cumulate overturn has primarily focused upon the behavior of ilmenite-bearing cumulates; however, the behavior of KREEP during such a process is unclear. Against these uncertainties, it is evident that new data on the KREEP elements (e.g., Th and Sm) in pyroclastic glasses can aid in unraveling the inventory and distribution of heat-producing elements in the lunar mantle.

3. Analytical approach

Several pyroclastic glasses were analyzed by ion microprobe: Apollo 11 (A11) orange and green glasses, Apollo 12 (A12) red glasses, Apollo 14 (A14) red, black, orange, yellow, and green (types A and B) glasses, Apollo 15 (A15) yellow, red, and green (types A–E) glasses, and Apollo 17 (A17) orange, yellow, and green glasses (see Delano, 1979 for classification scheme). Lunar pyroclastic glasses are commonly categorized based on their TiO_2 concentrations (Shearer and Papike, 1993). Like the mare basalts, lunar pyroclastic glasses exhibit TiO_2 concentrations that range from 0.2 to 17.0 wt% (Shearer and Papike, 1993). We use the following classification scheme to distinguish the glasses from another: very low-Ti (VLT) = 0.2–1.0 wt% TiO_2 , low-Ti = 1.0–3.4 wt% TiO_2 , intermediate-Ti = 3.4–6.9 wt% TiO_2 , high-Ti = 8.6–14.0 wt% TiO_2 , and very high-Ti (VHT) = 14.0–17.0 wt% TiO_2 . It is apparent that there is a strong correlation between the color of the glasses and their TiO_2 content. For example, the red-black

glasses have very high TiO_2 concentrations, the orange and red glasses have high TiO_2 concentrations, the yellow glasses have intermediate TiO_2 concentrations, and the green glasses have low to very low TiO_2 concentrations (see Delano, 1979; Shearer and Papike, 1993).

Thorium and samarium concentrations in the lunar pyroclastic glasses were measured using a Cameca ims 4f secondary ion mass spectrometer (SIMS) located at the University of New Mexico. Primary O^- ions were accelerated through a nominal potential of 10 kV. A primary beam current of 15 nA was focused on the sample over a spot diameter of 10–15 μm . Sputtered secondary ions were energy-filtered using a sample-offset voltage of 105 V and an energy window of ± 25 V. Concentrations of thorium and samarium were calculated using empirical relationships of $^{147}\text{Sm}/^{30}\text{Si}^+$ and $^{232}\text{Th}/^{30}\text{Si}^+$. These ratios were normalized to SiO_2 concentrations derived from electron microprobe analyses.

Measured intensities from the SIMS were calibrated against known concentrations in six glass standards that contain a range of Th and Sm abundances (Table 1). The strength of this analytical technique is that SIMS is capable of obtaining in situ analyses on polished thin sections at a high spatial resolution (10–50 μm). Intensity-to-concentration ratios for Th and Sm in the basaltic glass standards were reproducible to within $\pm 2\%$ during the 14 analytical sessions in this study. The major element analyses of these glasses were previously documented in other studies (see Delano, 1979; Shearer and Papike, 1993; Papike et al., 1998).

4. Analytical results

Results from this study show that the lunar pyroclastic glasses have a wide range of thorium and samarium concentrations, with Th ranging from 0.20 to 5.6 ppm and Sm ranging from 0.87 to 21 ppm (Table 2 and Fig. 1). Low and very low-Ti (VLT) compositions, represented by green pyroclastic glasses, have the lowest concentrations of both Th and Sm (Fig. 1). Intermediate-Ti basalts, represented by yellow glasses, overlap slightly with the low-Ti and VLT basalts in Th content but have higher Sm concentrations. High-Ti basalts, represented by the orange, red, and black glasses, have even higher Sm concentrations and overlap the intermediate-Ti glasses in Th content. The very high-Ti glasses (A14 red-black

glasses) have characteristically high concentrations of Th. All glasses from the Apollo 14 site have Th and Sm concentrations that fall along a trend that includes the Th and Sm concentrations of urKREEP (e.g., Shearer et al., 1990, 1991).

A plot of Th/Sm versus Th (Fig. 2) shows that the VLT, the very high-Ti, and some of the intermediate-Ti samples have similar Th/Sm ratios (ranging from 0.2 to 0.4). However, all of the high-Ti samples and one of the intermediate-Ti samples have Th/Sm ratios that differ significantly from the other compositional types (i.e., Th/Sm < 0.1) (Fig. 2). The A14 very high-Ti glasses stand out because of their high Th content relative to glasses from the other landing sites (e.g., Shearer and Papike, 1993). The Th and Sm concentrations of all of the pyroclastic glasses are high relative to CI chondrites, which have 0.029 ppm Th, 0.147 ppm Sm, and a Th/Sm ratio of 0.20 (i.e., Anders and Grevesse, 1989). The VLT and A14 high-Ti glasses have Th and Sm concentrations that fall on a mixing line between the CI chondrite and urKREEP values (Figs. 1 and 2).

Previous studies of bulk fragments from the lunar sample suite reveal that there are predictable relationships between Th, U, and K in lunar samples (e.g., Korotev, 1998). For instance, Korotev (1998) showed that U and K concentrations in lunar samples can be calculated using the following equations:

$$\text{U} = (\text{Th} \times 0.2725) - 0.001.$$

$$\text{K} = (\text{Th} \times 397) + 154.$$

We use these equations to estimate the U and K concentrations for each of the pyroclastic glasses that were analyzed in this study (Table 2).

5. Discussion

High-pressure experiments indicate that the temperatures and pressures of multiple saturation for pyroclastic glasses are located at 1410–1560 °C and 1.7–2.5 GPa (Stolper et al., 1974; Green et al., 1975; Delano, 1980; Chen et al., 1982; Chen and Lindsley, 1983; Longhi, 1992; Elkins-Tanton et al., 2000, 2003). If the point of multiple saturation represents the minimum depth of melting, then the basaltic magmas represented by the pyroclastic glasses were generated at depths ≥ 400 km (Papike et al., 1998; Hess, 2000). A deep mantle origin for the lunar pyroclastic glasses is supported by the duration of mare volcanism, which requires

Table 1
Standards used for SIMS calibration

Standard	Type	Sm (ppm)	Th (ppm)	Source
AII93-11-103	Basaltic glass	3.28	102	Dr. Klaus Jochum, Max-Plank-Institut fur Chemie
AH83-KL2	Basaltic glass	5.7	1.1	Dr. Klaus Jochum, Max-Plank-Institut fur Chemie
AH83-ML3B	Basaltic glass	4.9	56	Dr. Klaus Jochum, Max-Plank-Institut fur Chemie
ATHO	Rhyolitic glass	15	7.4	Dr. Klaus Jochum, Max-Plank-Institut fur Chemie
WU-A	Synthetic glass	5.73	0.06	Dr. Brad Jolliff, Washington University
WU-B	Synthetic glass	—	8.65	Dr. Brad Jolliff, Washington University

Table 2

Results from SIMS of analyses of lunar pyroclastic glasses

Apollo site	Sample number	Glass color	Th (ppm)	Sm (ppm)	Th/Sm	U ^a (ppm)	K ^a (wt.%)
A11	10030g2	Orange	0.52	9.0	0.058	0.14	0.036
A11	10030g3	Orange	0.53	10.1	0.052	0.14	0.036
A11	10030g4	Orange	0.60	9.3	0.065	0.16	0.039
A11	10030g7	Orange	0.48	10.1	0.048	0.13	0.034
A11	10030g8	Orange	0.56	9.8	0.057	0.15	0.038
A11	10030g12	Orange	0.41	8.3	0.050	0.11	0.032
A11	10030g13	Orange	0.61	9.5	0.064	0.17	0.040
A11	10030g14	Orange	0.61	9.2	0.066	0.16	0.040
A11	10031g1	Orange	0.43	8.6	0.051	0.12	0.033
A11	10031g2	Orange	0.44	8.7	0.051	0.12	0.033
A11	10031g3	Orange	0.52	7.6	0.069	0.14	0.036
A11	10031g4	Orange	0.54	9.0	0.060	0.15	0.037
A11	10031g9	Orange	0.55	8.8	0.062	0.15	0.037
A11	10031g11	Orange	0.45	9.1	0.050	0.12	0.033
A11	10031g13	Orange	0.43	8.7	0.049	0.12	0.032
A11	10031g17	Orange	0.43	8.0	0.054	0.12	0.032
A11	10031g18	Orange	0.61	9.6	0.063	0.16	0.040
A11	10031g19	Orange	0.51	10.0	0.051	0.14	0.036
A11	10031g22	Orange	0.59	9.1	0.064	0.16	0.039
Average			0.52	9.1	0.057	0.14	0.04
1σ			0.069	0.698	0.007	0.019	0.003
A12	12033g1	Red	1.1	12.9	0.082	0.29	0.058
A12	12033g3	Red	1.2	13.3	0.092	0.33	0.064
A12	12033g4	Red	1.2	12.7	0.093	0.32	0.062
A12	12033g5	Red	1.3	13.0	0.102	0.36	0.068
A12	12033g6	Red	1.0	11.6	0.089	0.28	0.056
A12	12033g11	Red	1.1	12.3	0.091	0.30	0.060
A12	12033g8	Red	1.1	12.4	0.087	0.29	0.058
A12	12033g13	Red	1.1	12.1	0.092	0.30	0.060
A12	12033g14	Red	1.2	12.4	0.093	0.31	0.061
Average			1.1	12.6	0.091	0.31	0.06
1 σ			0.092	0.517	0.005	0.025	0.004
A14	14048g75	Green	0.68	3.2	0.21	0.18	0.042
A14	14048g71	Green	1.0	4.0	0.25	0.27	0.055
A14	14048g52	Green	0.45	2.1	0.21	0.12	0.033
A14	14048g32	Green	1.2	5.2	0.24	0.34	0.065
A14	14049g17	Green	0.58	2.3	0.26	0.16	0.038
A14	14049g18	Green	1.1	4.8	0.24	0.31	0.061
A14	14049g03	Green	1.4	5.5	0.25	0.37	0.069
A14	14049g11	Green	1.4	5.4	0.25	0.37	0.070
Average			1.0	4.0	0.24	0.26	0.05
1 σ			0.364	1.373	0.018	0.098	0.014
A14	14041g34	Red	3.9	16	0.24	1.04	0.169
A14	14041g34b	Red	4.3	16	0.28	1.17	0.188
A14	14301g3	Red	5.6	21	0.26	1.52	0.238
A14	14301g5	Black	3.2	15	0.22	0.86	0.142
A14	14048g30	Red	3.4	14	0.24	0.91	0.149
Average			4.1	16	0.25	1.10	0.18
1 σ			0.967	2.886	0.023	0.261	0.038
A15	15041g30	Yellow	1.3	7.9	0.17	0.36	0.068
A15	15318g1	Yellow	1.2	7.0	0.17	0.31	0.062
A15	15030g5	Yellow	0.50	5.9	0.084	0.13	0.035
A15	15030g6	Yellow	0.50	5.8	0.086	0.13	0.035
A15	15049g23	Yellow	1.5	7.2	0.20	0.40	0.074
Average			1.0	6.8	0.14	0.27	0.05
1 σ			0.465	0.915	0.054	0.126	0.018
A15	15426,18g3	Red	1.1	13	0.090	0.31	0.061
A15	15426,18g2	Red	1.2	14	0.084	0.31	0.061

Table 2 (continued)

Apollo site	Sample number	Glass color	Th (ppm)	Sm (ppm)	Th/Sm	U ^a (ppm)	K ^a (wt.%)
A15	15426,18g1	Red	1.3	14	0.091	0.34	0.066
A15	15318g30	Red	1.4	14	0.10	0.37	0.070
Average 1 σ			1.2	14	0.091	0.33	0.06
			0.110	0.557	0.007	0.030	0.004
A15	15318g5	Green A	0.28	1.2	0.24	0.077	0.027
A15	15318g6	Green A	0.30	1.3	0.23	0.081	0.027
A15	15427g1	Green A	0.49	1.4	0.34	0.13	0.035
A15	15427g2	Green A	0.49	1.4	0.34	0.13	0.035
A15	15041g33	Green A	0.21	0.90	0.23	0.056	0.024
A15	15426,18g28	Green A	0.20	1.0	0.20	0.053	0.023
A15	15426,18g27	Green A	0.20	0.87	0.23	0.055	0.023
A15	15426,18g21	Green A	0.21	0.93	0.22	0.056	0.024
A15	15426,18g20	Green A	0.21	0.91	0.23	0.057	0.024
A15	15318g40	Green B	0.34	1.5	0.23	0.091	0.029
A15	15427g1	Green B	0.37	1.5	0.24	0.099	0.030
A15	15427g2	Green B	0.37	1.5	0.24	0.100	0.030
A15	15318g33	Green D	0.32	1.5	0.21	0.09	0.028
A15	15318g29	Green D	0.29	1.3	0.22	0.079	0.027
A15	15318g31	Green D	0.33	1.4	0.24	0.089	0.028
A15	15427g1	Green D	0.24	1.1	0.23	0.065	0.025
A15	15427g2	Green D	0.32	1.3	0.25	0.085	0.028
A15	15426,18g23	Green D	0.21	1.0	0.22	0.056	0.024
A15	15426,18g11	Green D	0.30	1.1	0.28	0.081	0.027
A15	15426,18g22	Green D	0.28	1.2	0.24	0.076	0.027
A15	15426,18g17	Green D	0.30	1.4	0.22	0.081	0.027
A15	15426,18g26	Green D	0.22	0.93	0.24	0.061	0.024
A15	15318g7	Green E	0.34	1.4	0.25	0.093	0.029
A15	15318g32	Green E	0.47	1.9	0.25	0.13	0.034
A15	15426,18g25	Green E	0.32	1.2	0.27	0.086	0.028
Average 1 σ			0.30	1.2	0.24	0.082	0.027
			0.086	0.263	0.033	0.023	0.003
A17	79135g19	Yellow	1.1	6.8	0.16	0.30	0.059
A17	79135g20	Green	0.73	2.5	0.29	0.20	0.044
A17	79135g21	Green	0.63	1.9	0.33	0.17	0.040
A17	79135g27	Green	0.42	2.0	0.21	0.11	0.032
A17	79135g68	Green	0.42	1.8	0.24	0.11	0.032
Average for A17 green glasses 1 σ			0.55	2.1	0.26	0.15	0.04
			0.155	0.328	0.054	0.042	0.006
A17	79315g1	Orange	0.54	8.0	0.068	0.15	0.037
A17	79315g2	Orange	0.51	8.2	0.062	0.14	0.036
A17	79315g3	Orange	0.56	8.3	0.067	0.15	0.037
A17	79315g4	Orange	0.57	8.1	0.070	0.15	0.038
A17	79315g5	Orange	0.56	8.4	0.067	0.15	0.038
A17	79315g6	Orange	0.47	7.8	0.060	0.13	0.034
Average 1 σ			0.53	8.1	0.066	0.14	0.04
			0.039	0.219	0.004	0.010	0.002

^a Calculated from equation of Korotev (1998).

heat sources that were long-lived and therefore deep within the Moon (Hess, 2000).

Many petrologic models predict that the source regions for the volcanic glasses underwent small to moderate degrees of partial melting (3–15%), which left behind a residue of olivine and orthopyroxene (Binder, 1982; Unruh et al., 1984; Hughes et al., 1988; Longhi, 1992; Snyder et al., 1992; Shearer et al., 1991; Shearer and Papike,

1993). The most common estimates of partial melting range between 4% and 10% (e.g., Hughes et al., 1988; Shearer et al., 1991; Shearer and Papike, 1993). Basaltic melts were transported to the lunar surface by one of at least two different methods. One model proposes that basaltic magmas were produced by relatively slow, polybaric melting in a large diapir (see Longhi, 1987, for discussion). Another model suggests that the ascending magma body was

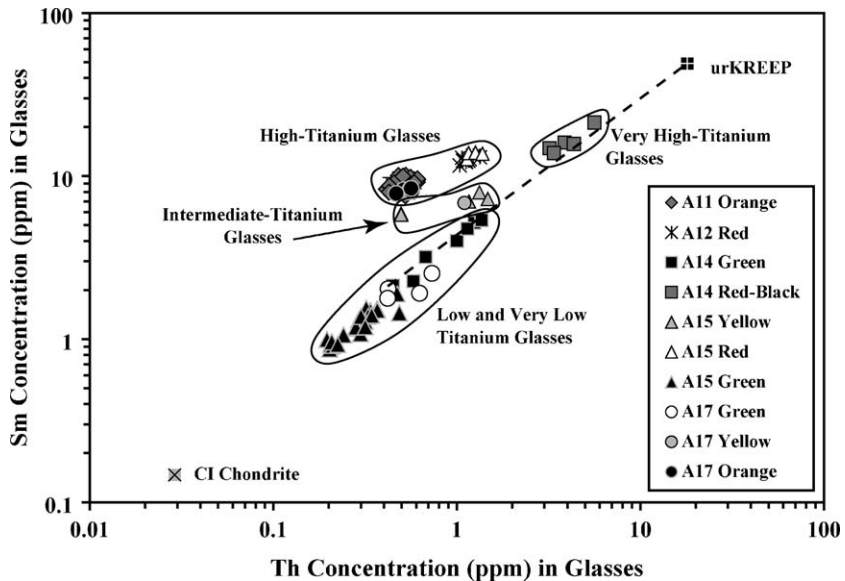


Fig. 1. Plot of measured concentrations for Sm and Th in the lunar pyroclastic glasses. Note that the very high-Ti glasses from the Apollo 14 site plot on a mixing line between urKREEP and the A14 very low-Ti glasses. Error bars are equal to or smaller than the size of the symbols. The Th and Sm concentrations of CI chondrites (Anders and Grevesse, 1989) and urKREEP (Warren and Wasson, 1979) are plotted for comparison.

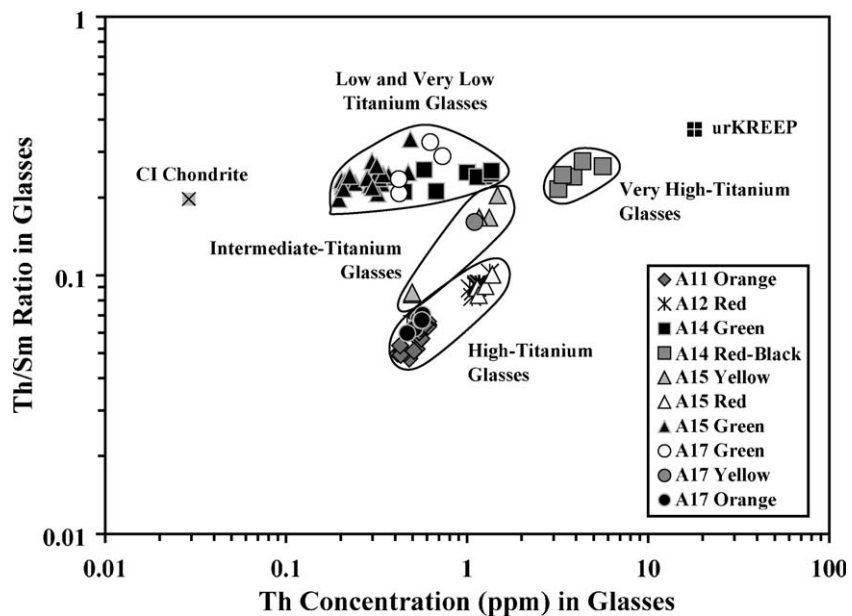


Fig. 2. Plot of Th/Sm versus measured Th concentrations in lunar pyroclastic glasses. The Th/Sm ratios of the very high-Ti glasses are distinctly different than the ratios in the high-Ti glasses. Error bars are equal to or smaller than the size of the symbols. The Th and Sm concentrations of CI chondrites (Anders and Grevesse, 1989) and urKREEP (Warren and Wasson, 1979) are plotted for comparison.

transported rapidly to the lunar surface, did not experience significant fractionation or assimilation, and therefore retained the composition of the primary melt (Hess, 2000; Wilson and Head, 2003; Beck et al., 2006). Regardless of which transport model prevails, it is apparent that a record of mantle heterogeneity is preserved within the lunar pyroclastic glasses.

The relatively primitive compositions of the pyroclastic glasses (i.e., high molar Mg/(Mg + Fe)) indicate that lunar pyroclastic glasses represent the closest approximations of

unmodified melts from the lunar mantle (Shearer and Papike, 1993). The importance of the pyroclastic glasses is amplified by the observation that all of the glasses were produced by similar degrees of partial melting (Binder, 1982; Delano, 1986). Therefore, any compositional differences among the glasses will reflect compositional differences between the source regions, not different degrees of partial melting. Given this information, the results from this study can be used to address: (1) the Th and Sm concentrations of basaltic source regions, (2) heat production

in the lunar mantle, and (3) the bulk Th and Sm composition of the lunar mantle.

5.1. Th–Sm concentrations in the pyroclastic glass source regions

We calculated the Th and Sm concentrations of the source regions for the pyroclastic glasses using the batch melting equation:

$$C_o = (C_l \times F) \text{ when } D \cong 0.$$

Here, C_o = concentration of a given element in the source, C_l = concentration of a given element in the liquid, F = fraction of melt, and D = bulk mineral–melt distribution coefficient. For the source calculations, the bulk D -values for Th and Sm are essentially zero for the residual mineralogy (see Tables 3a and 3b), as long as it is assumed that the residual mineralogy consists of olivine and orthopyroxene (e.g., Longhi, 1992 and references therein). Given this assumption, the SIMS data from this study can be used, in conjunction with the above equation, to calculate source compositions for the pyroclastic glasses at various degrees of partial melting ($F = 5\%, 10\%, 15\%$); however, our preferred value of partial melting is 10%, which is consistent with the studies of Hughes et al. (1988), Shearer

et al. (1991), and Shearer and Papike (1993). Our calculated source compositions can be found in Tables 4, A1, and A2.

The calculated source compositions discussed in this study are valid if: (1) basaltic magmas were produced by batch melting, (2) the residuum left behind after melting consisted of olivine and orthopyroxene, (3) the basaltic magmas were generated by 5–15% partial melting, and (4) trace-element partition coefficients used in the calculations are appropriate for the assumed temperature, pressure, and composition of the basaltic melts. These assumptions are compromised to some extent by several variables, including: the ratio of olivine to orthopyroxene in the residuum, the extent to which the basaltic magmas deviate from primary magma compositions, and whether a static model is applicable rather than a dynamic polybaric melting model (Longhi, 1992; Shearer and Papike, 1993). Fortunately, most of these complications do not drastically affect the behavior or distribution of Th or Sm during the petrogenesis of the lunar pyroclastic glasses. For instance, if the mineral assemblage of the residuum is changed from 80% olivine and 20% orthopyroxene to 50% olivine and 50% orthopyroxene, the respective bulk D -values for Th change only slightly, from 0.05 to 0.08. The major source of error in these

Table 3a
List of partition coefficients used by Snyder et al. (1992)

	D_{Th}	D_{Sm}	0-40 PCS	40-78 PCS	78-86 PCS	86-95 PCS	95-99 PCS
Olivine	0.03	0.0006	100%	25%	25%	—	—
Orthopyroxene	0.13	0.022	—	75%	—	—	—
Plagioclase	0.0208	0.017	—	—	53%	36%	31%
Pigeonite	0.13	0.011	—	—	22%	26%	38%
Clinopyroxene	0.13	0.17	—	—	—	38%	24%
Ilmenite	0.55	0.0023	—	—	—	—	11%
Bulk D_{Th}	—	—	0.03	0.11	0.05	0.09	0.14
Bulk D_{Sm}	—	—	0.0006	0.017	0.01	0.07	0.05

PCS, percent crystalline solid (Snyder et al., 1992).

Table 3b
List of bulk partition coefficients used in this study

	D_{Th}	D_{Sm}	0-40 PCS	40-78 PCS	78-86 PCS	86-95 PCS	95-99 PCS
Olivine	0.0001 ^a	0.0001 ^b	100%	25%	25%	—	—
Orthopyroxene	0.001 ^a	0.008 ^c	—	75%	—	—	—
Plagioclase	0.0208 ^d	0.017 ^d	—	—	53%	36%	31%
Pigeonite	0.0038 ^e	0.011 ^f	—	—	22%	26%	38%
Clinopyroxene	0.00026 ^a	0.26 ^a	—	—	—	38%	24%
Ilmenite	0.00055 ^g	0.00059 ^g	—	—	—	—	11%
Bulk D_{Th}	—	—	0.0001	0.0008	0.01	0.01	0.01
Bulk D_{Sm}	—	—	0.0001	0.006	0.01	0.11	0.07

PCS, percent crystalline solid (Snyder et al., 1992).

^a McKenzie and O’Nions (1991).

^b Beattie (1994).

^c Schwandt and McKay (1998).

^d Phinney and Morrison (1990).

^e Landwehr et al. (2001).

^f McKay et al. (1986).

^g Zack and Brumm (1998).

Table 4

Calculated compositions of pyroclastic glass source regions, assuming 10% partial melting

Apollo site	Sample number	Glass color	Th (ppm)	Sm (ppm)	Th/Sm	U (ppm)	K (wt.%)	A ($\mu\text{W}/\text{m}^3$)
A11	10030g2	Orange	0.052	0.90	0.058	0.014	0.017	0.042
A11	10030g3	Orange	0.053	1.0	0.052	0.014	0.017	0.046
A11	10030g4	Orange	0.060	0.93	0.065	0.016	0.018	0.045
A11	10030g7	Orange	0.048	1.0	0.048	0.013	0.017	0.045
A11	10030g8	Orange	0.056	0.98	0.057	0.015	0.018	0.045
A11	10030g12	Orange	0.041	0.83	0.050	0.011	0.017	0.038
A11	10030g13	Orange	0.061	0.95	0.064	0.017	0.018	0.045
A11	10030g14	Orange	0.061	0.92	0.066	0.016	0.018	0.044
A11	10031g1	Orange	0.043	0.86	0.051	0.012	0.017	0.039
A11	10031g2	Orange	0.044	0.87	0.051	0.012	0.017	0.039
A11	10031g3	Orange	0.052	0.76	0.069	0.014	0.017	0.037
A11	10031g4	Orange	0.054	0.90	0.060	0.015	0.018	0.042
A11	10031g9	Orange	0.055	0.88	0.062	0.015	0.018	0.042
A11	10031g11	Orange	0.045	0.91	0.050	0.012	0.017	0.041
A11	10031g13	Orange	0.043	0.87	0.049	0.012	0.017	0.039
A11	10031g17	Orange	0.043	0.80	0.054	0.012	0.017	0.037
A11	10031g18	Orange	0.061	0.96	0.063	0.016	0.018	0.046
A11	10031g19	Orange	0.051	1.0	0.051	0.014	0.017	0.045
A11	10031g22	Orange	0.059	0.91	0.064	0.016	0.018	0.043
Average			0.052	0.91	0.057	0.014	0.017	0.042
1σ			0.007	0.070	0.007	0.002	0.000	0.003
A12	12033g1	Red	0.11	1.3	0.082	0.029	0.020	0.065
A12	12033g3	Red	0.12	1.3	0.092	0.033	0.020	0.069
A12	12033g4	Red	0.12	1.3	0.093	0.032	0.020	0.066
A12	12033g5	Red	0.13	1.3	0.102	0.036	0.021	0.070
A12	12033g6	Red	0.10	1.2	0.089	0.028	0.020	0.060
A12	12033g11	Red	0.11	1.2	0.091	0.030	0.020	0.064
A12	12033g8	Red	0.11	1.2	0.087	0.029	0.020	0.064
A12	12033g13	Red	0.11	1.2	0.092	0.030	0.020	0.063
A12	12033g14	Red	0.12	1.2	0.093	0.031	0.020	0.065
Average			0.11	1.3	0.091	0.031	0.020	0.065
1σ			0.009	0.052	0.005	0.002	0.000	0.003
A14	14048g75	Green	0.068	0.32	0.21	0.018	0.018	0.025
A14	14048g71	Green	0.10	0.40	0.25	0.027	0.019	0.033
A14	14048g52	Green	0.045	0.21	0.21	0.012	0.017	0.017
A14	14048g32	Green	0.12	0.52	0.24	0.034	0.020	0.042
A14	14049g17	Green	0.058	0.23	0.26	0.016	0.018	0.020
A14	14049g18	Green	0.11	0.48	0.24	0.031	0.020	0.038
A14	14049g03	Green	0.14	0.55	0.25	0.037	0.021	0.045
A14	14049g11	Green	0.14	0.54	0.25	0.037	0.021	0.044
Average			0.10	0.40	0.24	0.026	0.019	0.033
1σ			0.036	0.137	0.018	0.010	0.001	0.011
A14	14041g34	Red	0.39	1.6	0.24	0.10	0.031	0.125
A14	14041g34b	Red	0.43	1.6	0.28	0.12	0.033	0.132
A14	14301g3	Red	0.56	2.1	0.26	0.15	0.038	0.174
A14	14301g5	Black	0.32	1.5	0.22	0.086	0.028	0.109
A14	14048g30	Red	0.34	1.4	0.24	0.091	0.029	0.109
Average			0.41	1.6	0.25	0.110	0.032	0.130
1σ			0.097	0.289	0.023	0.026	0.004	0.027
A15	15041g30	Yellow	0.13	0.79	0.17	0.036	0.021	0.052
A15	15318g1	Yellow	0.12	0.70	0.17	0.031	0.020	0.046
A15	15030g5	Yellow	0.05	0.59	0.084	0.013	0.017	0.031
A15	15030g6	Yellow	0.05	0.58	0.086	0.013	0.017	0.030
A15	15049g23	Yellow	0.15	0.72	0.20	0.040	0.021	0.053
Average			0.10	0.68	0.14	0.027	0.019	0.043
1σ			0.046	0.091	0.054	0.013	0.002	0.011
A15	15426,18g3	Red	0.11	1.3	0.090	0.031	0.020	0.065
A15	15426,18g2	Red	0.12	1.4	0.084	0.031	0.020	0.070

Table 4 (continued)

Apollo site	Sample number	Glass color	Th (ppm)	Sm (ppm)	Th/Sm	U (ppm)	K (wt.%)	A ($\mu\text{W}/\text{m}^3$)
A15	15426,18g1	Red	0.13	1.4	0.091	0.034	0.020	0.072
A15	15318g30	Red	0.14	1.4	0.10	0.037	0.021	0.073
Average 1σ			0.12 0.011	1.4 0.056	0.091 0.007	0.033 0.003	0.020 0.000	0.070 0.003
A15	15318g5	Green A	0.028	0.12	0.24	0.008	0.017	0.011
A15	15318g6	Green A	0.030	0.13	0.23	0.008	0.017	0.012
A15	15427g1	Green A	0.049	0.14	0.34	0.013	0.017	0.015
A15	15427g2	Green A	0.049	0.14	0.34	0.013	0.017	0.015
A15	15041g33	Green A	0.021	0.090	0.23	0.006	0.016	0.009
A15	15426,18g28	Green A	0.020	0.10	0.20	0.005	0.016	0.009
A15	15426,18g27	Green A	0.020	0.087	0.23	0.005	0.016	0.008
A15	15426,18g21	Green A	0.021	0.093	0.22	0.006	0.016	0.009
A15	15426,18g20	Green A	0.021	0.091	0.23	0.006	0.016	0.009
A15	15318g40	Green B	0.034	0.15	0.23	0.009	0.017	0.013
A15	15427g1	Green B	0.037	0.15	0.24	0.010	0.017	0.014
A15	15427g2	Green B	0.037	0.15	0.24	0.010	0.017	0.013
A15	15318g33	Green D	0.032	0.15	0.21	0.009	0.017	0.013
A15	15318g29	Green D	0.029	0.13	0.22	0.008	0.017	0.011
A15	15318g31	Green D	0.033	0.14	0.24	0.009	0.017	0.012
A15	15427g1	Green D	0.024	0.11	0.23	0.007	0.016	0.010
A15	15427g2	Green D	0.032	0.13	0.25	0.009	0.017	0.012
A15	15426,18g23	Green D	0.021	0.10	0.22	0.006	0.016	0.009
A15	15426,18g11	Green D	0.030	0.11	0.28	0.008	0.017	0.011
A15	15426,18g22	Green D	0.028	0.12	0.24	0.008	0.017	0.011
A15	15426,18g17	Green D	0.030	0.14	0.22	0.008	0.017	0.012
A15	15426,18g26	Green D	0.022	0.093	0.24	0.006	0.016	0.009
A15	15318g7	Green E	0.034	0.14	0.25	0.009	0.017	0.013
A15	15318g32	Green E	0.047	0.19	0.25	0.013	0.017	0.017
A15	15426,18g25	Green E	0.032	0.12	0.27	0.009	0.017	0.011
Average 1σ			0.030 0.009	0.12 0.026	0.24 0.033	0.008 0.002	0.017 0.000	0.011 0.002
A17	79135g19	Yellow	0.11	0.68	0.16	0.030	0.020	0.045
A17	79135g20	Green	0.073	0.25	0.29	0.020	0.018	0.023
A17	79135g21	Green	0.063	0.19	0.33	0.017	0.018	0.019
A17	79135g27	Green	0.042	0.20	0.21	0.011	0.017	0.016
A17	79135g68	Green	0.042	0.18	0.24	0.011	0.017	0.015
Average for A17 green glasses 1σ			0.055 0.015	0.21 0.033	0.26 0.054	0.015 0.004	0.018 0.001	0.019 0.004
A17	79315g1	Orange	0.054	0.80	0.068	0.015	0.018	0.039
A17	79315g2	Orange	0.051	0.82	0.062	0.014	0.017	0.039
A17	79315g3	Orange	0.056	0.83	0.067	0.015	0.018	0.040
A17	79315g4	Orange	0.057	0.81	0.070	0.015	0.018	0.040
A17	79315g5	Orange	0.056	0.84	0.067	0.015	0.018	0.041
A17	79315g6	Orange	0.047	0.78	0.060	0.013	0.017	0.037
Average 1σ			0.053 0.004	0.81 0.022	0.066 0.004	0.014 0.001	0.018 0.000	0.039 0.001

calculations involves the use of incorrect trace-element partition coefficients (D -values) and the subsequent calculation of bulk D -values for the pertinent mineral assemblages. Therefore, we evaluated the mineral–melt D -values and bulk D -values used by previous authors (i.e., Snyder et al., 1992) and provide a slightly revised set of D - and bulk D -values for specific minerals in tholeiitic basalts (Tables 3a and 3b). It should be noted that differences in the bulk D -values are minor and that all

reasonable bulk D -values result in high mineral/melt concentrations.

Table 3a shows the trace-element partition coefficients (D -values) reported by Snyder et al. (1992) and Table 3b shows the updated partition coefficients that were used in this study. There is at least one major difference between the D -values used by Snyder et al. (1992) and those used in this study. For example, Snyder et al. (1992) report a D -value for Th in ilmenite of 0.55 (Table 3a) and we report

a D -value of 0.00055 (Table 3b). The D_{Th} value used by Snyder et al. (1992) is taken from Villemant et al. (1981), who analyzed ilmenite grains in alkali basalts from the Massif Central in France. Villemant et al. (1981) state that the D -value for Th in ilmenite is surprisingly high in their study. In fact, the D -value is so high that Villemant et al. (1981) conclude that the D -value probably represents the incorporation of mineral defects and/or trapped liquids. For comparison, we use the D_{Th} value of Zack and Brumm (1998), who use five different ilmenite-liquid pairs from a variety of locations to arrive at a D_{Th} value of 0.00055. A comparison of Tables 3a and 3b shows that there are several other, more subtle differences between the values of Snyder et al. (1992) and the values we used (e.g., Table 3b). The D -values that we report in Table 3b were chosen because they are more recent and had a higher precision than those reported in Snyder et al. (1992). Many of the D -values reported by Snyder et al. (1992) were taken from much older references (e.g., Weill and McKay, 1975 and Villemant et al., 1981).

If we assume that all of the pyroclastic glasses were produced by 10% partial melting of their respective source regions (e.g., Binder, 1982; Unruh et al., 1984; Hughes et al., 1988; Longhi, 1987, 1992; Shearer et al., 1991; Shearer and Papike, 1993), we can calculate and compare the compositions of the source regions for each of the different glasses (Table 4 and Fig. 3). Comparison of Figs. 1 and 3 shows the extent to which the calculated compositions of the source regions differ from the concentrations measured in the pyroclastic glasses. The differences between the absolute concentrations in the sources and the melts are the result of small degrees of partial melting, a process that preferentially liberates incompatible elements and concentrates them in the melt (Hess, 1989). Fig. 3 shows that

the Th and Sm concentrations of CI chondrites (e.g., Anders and Grevesse, 1989) overlap with the Th and Sm concentrations of the calculated source regions for the low-Ti and VLT glasses.

The Th/Sm ratios of source regions for the VLT and low-Ti green glasses are close to the chondritic ratio of 0.20 (Fig. 4 and Table 5). The slightly higher ratios of the pyroclastic glasses may be attributed to trapped residual liquid in the cumulate source region (e.g., Snyder et al., 1992). The yellow, orange, A12 red, and A15 red glasses have relatively low Th/Sm ratios (Table 5). Based on these results one might predict that the very high-Ti A14 red-black glasses should also have low Th/Sm ratios; however, the average Th/Sm ratio of the A14 red-black glasses is 0.25 (Table 5). The Th/Sm ratio of the A14 red glasses can be explained if a cumulate source region with a Th/Sm ratio of 0.09 (i.e., the Th/Sm ratio of the source regions for the other red glasses) is mixed with a component that has a Th/Sm ratio of 0.37. We note that the urKREEP component calculated by Warren and Wasson (1979) has a Th/Sm ratio of 0.37, suggesting that the compositions of some of the source regions are consistent with the incorporation of urKREEP. This assertion is further supported by Figs. 3 and 4, which show that the calculated source regions for all of the Apollo 14 glasses plot on a mixing line with the urKREEP component. The potential mixing relationship correlates well with the findings of Shearer et al. (1989, 1990, 1991) and Shearer and Papike (1993), who showed that the Apollo 14 glasses are consistently REE enriched, have LREE enriched patterns, and have substantial negative Eu anomalies relative to other pyroclastic glasses. The chemical characteristics documented by Shearer et al. (1989, 1990, 1991) can be explained by two petrogenetic models, both of which involve KREEP

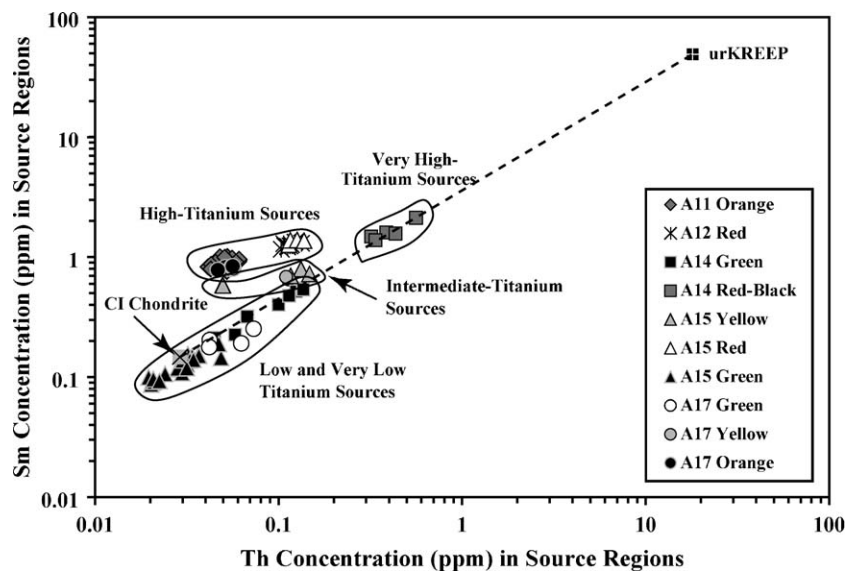


Fig. 3. Plot of calculated concentrations for Th and Sm in the source regions for the lunar pyroclastic glasses, assuming 10% partial melting. Note that the average CI chondrite composition of Anders and Grevesse (1989) plots in the same region as the low and very low-Ti glasses. The urKREEP composition of Warren and Wasson (1979) is plotted for comparison.

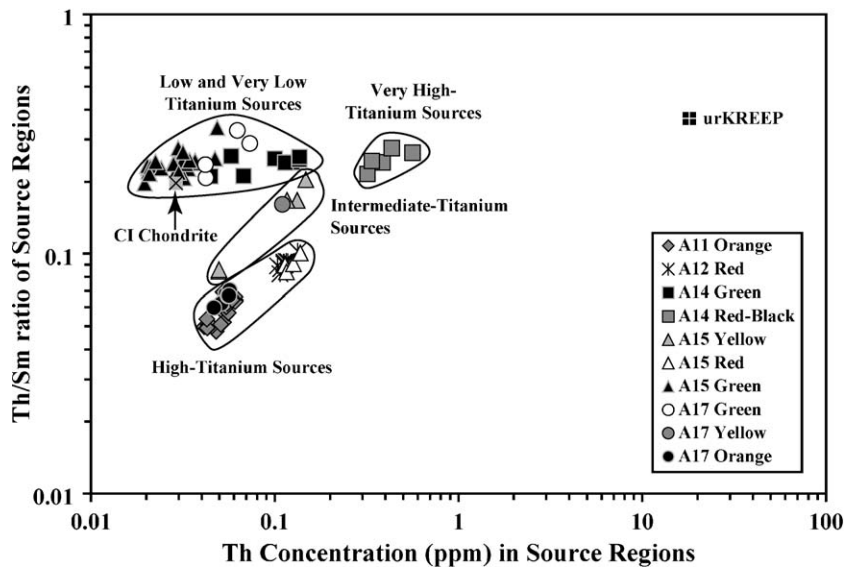


Fig. 4. Plot of Th/Sm versus calculated Th concentration in the source regions of the lunar pyroclastic glasses, assuming 10% partial melting. The sources for the high-Ti glasses and one of the intermediate-Ti glasses have Th/Sm ratios that are distinctly different than all of the other sources. The high Th content of the very high-Ti glasses could be explained by incorporation of the urKREEP component.

Table 5
Average Th/Sm ratios of source regions for selected glasses

Glass type	Th (ppm)	Sm (ppm)	Th/Sm
A14 Green (very low-Ti)	0.10	0.40	0.24
A15 Green (very low-Ti)	0.03	0.12	0.24
A17 Green (very low-Ti)	0.05	0.21	0.26
A15 Yellow (intermediate-Ti)	0.10	0.68	0.14
A17 Yellow (intermediate-Ti)	0.11	0.68	0.16
A17 Orange (high-Ti)	0.05	0.91	0.06
A11 Orange (high-Ti)	0.05	0.81	0.07
A12 Red (high-Ti)	0.11	1.26	0.09
A15 Red (high-Ti)	0.12	1.35	0.09
A14 Red (high-Ti)	0.41	1.63	0.25
Chondrite (Anders and Grevesse, 1989)	0.03	0.15	0.20
urKREEP (Warren and Wasson, 1979)	18	49	0.37

incorporation, albeit by two different processes within two different chemical and thermal regimes (Shearer et al., 1990).

The first petrogenetic model proposes that ascending basaltic magmas assimilated a KREEP component at the crust–mantle interface (see review by Shearer and Papike, 1993). The most significant obstacle to this model is that it requires assimilation of KREEP without significant modification of the major element characteristics of the glasses (Shearer et al., 1990). The thermal budget of assimilation generally induces significant crystallization (DePaolo, 1981), which would disrupt the linear arrays of major elements noted by Delano (1986), as well as the mixing relationship between the low-Ti and high-Ti components (Binder, 1982; Delano, 1986). The systematic increase in incompatible elements relative to Ti concentration, in conjunction with the lack of crystallization in the pyroclastic glasses, argues against KREEP assimilation in the A14

basaltic magmas (Shearer et al., 1990). It should be noted, however, that these chemical characteristics might also be explained if large volumes of hot urKREEP were assimilated by super-heated magmas (e.g., Wieczorek and Phillips, 2000).

The second petrogenetic model for incorporating KREEP into the Apollo 14 basaltic magmas involves addition of a KREEP component to the source region of the Apollo 14 magmas (see Hughes et al., 1990 and Shearer and Papike, 1993). The lack of correlation between TiO_2 content of the high-Ti mantle source, the Mg' (molar $\text{Mg}/(\text{Mg} + \text{Fe})$) of the mantle silicate residuum, and experimentally estimated depths of melting, lead to models that require hybridization of cumulate source regions (Shearer et al., 1990). These hybridization models require that the basaltic source regions consist of: (1) a primitive component of olivine and orthopyroxene, (2) an evolved component consisting of olivine, orthopyroxene, clinopyroxene, ilmenite, and plagioclase, and (3) an evolved KREEP-rich liquid (Shearer et al., 1990).

High-pressure experiments have shown that some of the KREEP-rich pyroclastic glasses were derived from depths ≥ 400 km (Chen et al., 1982; Chen and Lindsley, 1983; Longhi, 1992; Hess, 2000), implying that a KREEP component (along with heat-producing elements) had to be transported to the deep lunar mantle prior to the melting events. The existence of a KREEP component in the deep lunar mantle, along with a significant negative Eu anomaly in lunar basalts, argue for extensive mantle processing and convective overturn (e.g., Ringwood and Kesson, 1976; Hughes et al., 1990; Shearer et al., 1991; Spera, 1992; Hess and Parmentier, 1995). In total, the model for hybridized source regions explains the trace-element chemistry of the source regions while transporting heat-producing elements

to the deep lunar mantle, where they can serve as a source of heat for mantle melting.

Indirect information about the distribution of other heat-producing elements in the basaltic source regions can be obtained from known relationships between Th, U, and K in the lunar sample suite (e.g., Korotev, 1998). Given these relationships, we can use measured Th abundances to calculate the U and K concentrations in the source regions for the pyroclastic glasses (Tables 4, A1, and A2). It should be noted that the *D*-values for U and K in ilmenite are not well established and therefore the potential fractionation of U/Sm and K/Sm in the high-Ti glasses could vary from the relationships defined by Korotev (1998). Nevertheless, the results from this study provide estimates of the abundance, distribution, and heat-producing capabilities of Th, Sm, K, and U in the lunar mantle.

5.2. Heat production in the lunar mantle

Crater counting studies for young, but unsampled mare on the Moon, indicate that lunar mantle melting, expressed in the form of mare volcanism, may have persisted from >4 billion years ago until 1.1 billion years ago (Hiesinger et al., 2003). This prolonged period of basaltic magmatism implies that the thermal lifetime of the Moon was most likely extended by the decay of radioactive isotopes within the lunar mantle (e.g., Hess, 2000). Previous studies of the lunar mantle have suggested that heat flow in the mantle is strongly dependent on the abundances of three radioactive isotopes: Th, U, and K (Hsui, 1979; Warren and Rasmussen, 1987). However, the asymmetrical distribution of Th on the nearside of the Moon (e.g., Haskin, 1997; Haskin et al., 2000; Lawrence et al., 1998, 2000, 2003) indicates that Th, U, and K are not homogeneously distributed throughout the lunar mantle.

The amount of heat produced by radioactive elements in the lunar mantle can be calculated using the heat production equation of Buntebarth (1984) in conjunction with heat production constants calculated by Rybach (1988):

$$A(\mu\text{W/m}^3) = \rho \cdot \left[\sum(Q_i \cdot C_i) \right].$$

Here, ρ is the density of the lunar mantle (3340 kg/m³) (Schubert et al., 2001), Q_i is the heat production constant for element i , and C_i is the concentration of element i . The heat production constants for U, K, Th, and Sm are 9.52, 2.56, 3.48, and 1.03, respectively. The results of the heat production calculations for mantle models developed from 5%, 10%, and 15% partial melting, are shown in Tables 4, A1, and A2. The proportion of heat attributable to each of the above-mentioned elements, at a given concentration, is directly proportional to the heat production constants for those elements (i.e., U provides the greatest proportion of heat per unit concentration).

A plot of calculated heat production versus calculated Sm concentration in the source regions of the pyroclastic glasses (Fig. 5) shows the extent to which the source regions are capable of producing heat. The source regions for the high-Ti and intermediate-Ti basalts have intermediate concentrations of heat-producing elements and correspondingly intermediate heat production values. The source regions for the very low-Ti basalts have the lowest heat production values, whereas the source regions for the very high-Ti basalts have the highest (see Fig. 5).

We note that regions on the farside of the Moon do not appear to have KREEP-like concentrations of Th (Lawrence et al., 1998, 2000, 2003) and therefore may not have a significant KREEP component. If there were a significant KREEP component on the far side of the Moon, we would

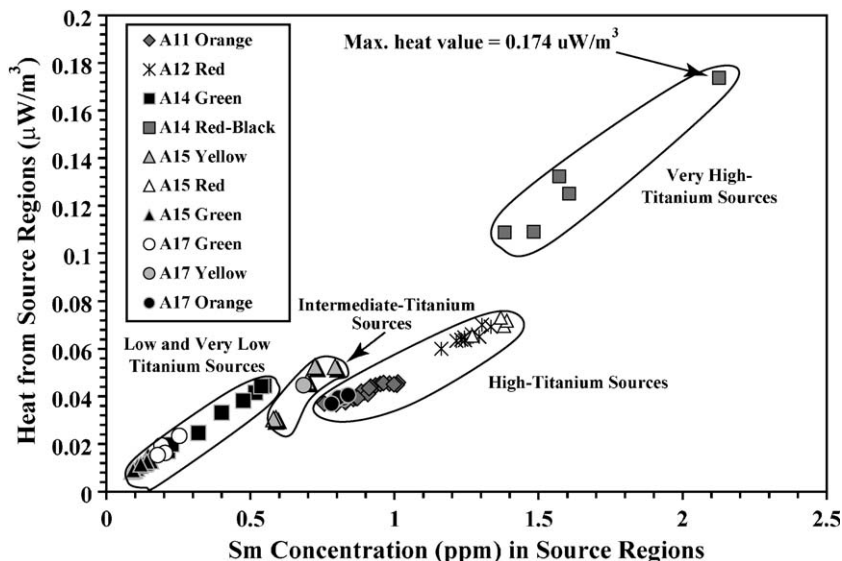


Fig. 5. Plot of calculated heat generated in source regions versus calculated Sm concentrations in the source regions. The source regions for the very high-Ti glasses generate the most heat.

expect to see evidence of KREEP in South Pole Aitken (SPA) basin. However, Lawrence et al. (2003) showed that the highest Th concentration measured in SPA is 2.5 ppm, which is much lower than the 11.7 ppm Th measured in the Procellarum KREEP Terrane (PKT, Jolliff et al., 2000). Therefore, we assume that the KREEP-poor VLT samples from this study represent the majority of the lunar mantle, especially compositions on the farside of the Moon. We also assume that the KREEP-rich samples from the Apollo 14 landing site represent maximum values for the nearside of the Moon.

We take the specific heat capacity of the lunar mantle to be 1.2 J/gK (Horai et al., 1970), which is equivalent to 0.00025 $\mu\text{W}/\text{m}^3 \text{K}$. Thus, 0.00025 μW are required to heat 1 m^3 of a given mantle assemblage by 1 K over a 500 million time period. Given these values, a high-Ti source region with an associated heat content of 0.174 $\mu\text{W}/\text{m}^3$ (i.e., the maximum in Fig. 5), will raise the temperature of 1 m^3 of mantle material by 683 K in 500 Ma. Conversely, a VLT (KREEP-poor) source region, with an associated heat flow of 0.073 $\mu\text{W}/\text{m}^3$, will raise the temperature of 1 m^3 of mantle material by only 287 K in 500 Ma (Fig. 6). A comparison of the maximum heat production values in Figs. 5 and 6 shows that heat production in a KREEP-rich source region is \sim 138% greater than heat production in a KREEP-poor source region (i.e., the farside of the Moon). The heat production values presented here are not meant to imply that these values are constant throughout the entire magmatic history of the Moon. In fact, the amount of heat production will decrease over time due to radioactive decay. However, the results from this study indicate that KREEP-rich and KREEP-poor source regions at one time had significantly different heat production capabilities. The difference in heat production between the near

and far sides of the Moon could be one of the reasons why there is an asymmetrical distribution of basaltic volcanism on the Moon.

5.3. Bulk composition of the lunar mantle

Previous estimates of the internal composition of the Moon have been based on experimental work (e.g., Green et al., 1971, 1975; Hedges and Kushiro, 1974; Kesson and Lindsley, 1974; Hess et al., 1975; Kesson, 1975; Longhi, 1987, 1992; Elkins-Tanton and Grove, 2001) as well as on measurements of mare basalt compositions (e.g., Ringwood and Essene, 1970; Smith et al., 1970; Rhodes and Hubbard, 1973; Duncan et al., 1976; Papike et al., 1976; Binder, 1982; Neal and Taylor, 1992). However, there are uncertainties associated with the use of basalt data, because it is debatable as to how Th, Sm, U, and K were acquired and what amounts of these elements were incorporated into mare basalts. Significant fractional crystallization of basaltic magmas may also fractionate Th from Sm. For these reasons, we propose that the Th and Sm concentrations of the rapidly erupted and relatively unfractionated lunar pyroclastic glasses are superior for determining the composition of the lunar mantle, at least until a direct sample from the lunar mantle can be obtained.

To calculate the Th and Sm composition of the lunar mantle, we assumed that there was whole Moon melting and that the LMO crystallized in the sequence proposed previously by Snyder et al. (1992). In their model, Snyder et al. (1992) suggest that the LMO crystallized to produce a low-Ti component (90–95% of the LMO), a high-Ti component (4–9% of the LMO), and a KREEP component (0.5–1% of the LMO). We assume that the average Th and Sm compositions of the green glasses represent the

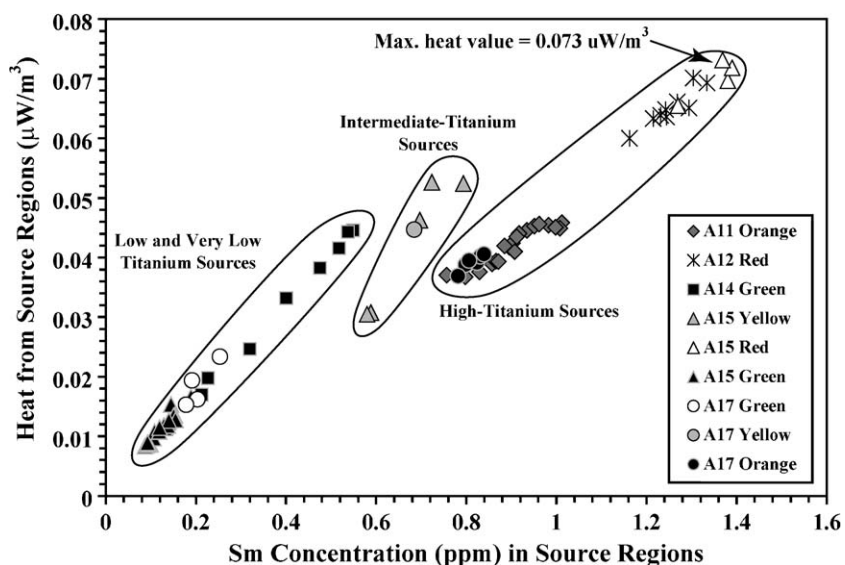


Fig. 6. Plot of calculated heat generated in source regions versus calculated Sm concentrations in the source regions. This plot does not contain data for the very high-Ti source regions, which represent Th-rich regions on the near side of the Moon. The maximum amount of heat generated by the intermediate-Ti sources is 58% less than that generated by the very high-Ti sources in Fig. 5.

Table 6
Bulk composition of the lunar mantle

Components	% Mantle ^a	Th (ppm)	Sm (ppm)	Th/Sm	U (ppm) ^b	K (ppm) ^b
Low-Ti avg. (based on 10% melting)	95	0.055	0.26	0.21	0.01	176
High-Ti avg. (based on 10% melting)	4.5	0.074	1.02	0.07	0.02	184
urKREEP (Warren and Wasson, 1979)	0.5	18	49	0.36	5.00	6900
Bulk Mantle (this study)		0.15	0.54	0.27	0.039	212
Jolliff et al. (2000) Mantle	—	0.04	—	—	—	—
Warren (2005) Mantle	—	0.025	—	—	—	—

^a Estimated by Snyder et al. (1992).

^b Calculated from equation of Korotev (1998).

average composition of the low-Ti component and that Th and Sm compositions of the orange and red-black glasses (not A14 glasses) represent the average composition of the high-Ti component (Table 6). We use the Th and Sm concentrations from Warren and Wasson (1979) to estimate the composition of the KREEP component. Table 6 shows our resulting estimate for the bulk composition of the lunar mantle, as well as a comparison of our estimates with previous studies. If the Th, U, and K relationships of Korotev (1998) are correct, we estimate that the bulk U composition of the lunar mantle is 0.039 ppm and the bulk K composition is 212 ppm. If the modeled distribution of mantle lithologies is not global, our estimate will be too high and if the actual degree of partial melting is higher or lower than we propose, our estimates will be correspondingly low or high. We realize that this model is greatly simplified. At the very least, the data from this study can be used to constrain future models that are more detailed.

6. Summary

In this paper, we use thorium and samarium data from lunar pyroclastic glasses to estimate the abundance of heat-producing elements in the source regions for high-Ti, intermediate-Ti, and very low-Ti pyroclastic glasses. These data show that the nearside lunar mantle is heterogeneous on a large scale with regard to heat-producing elements. In addition, the data show that areas of the deep lunar mantle (≥ 400 km) are enriched in a KREEP component. Heat-producing elements associated with KREEP provide a heat source for mantle melting and a driver for basaltic magmatism. KREEP-rich portions of the lunar mantle may have produced up to 138% more heat than KREEP-poor regions. The asymmetrical distribution of heat-producing elements might be one of the reasons for the abundance of magmatism on the nearside of the Moon.

Calculated Th/Sm ratios of the source regions for VLT, intermediate-Ti and the KREEP-rich high-Ti basalts are quite similar to one another and to values for CI chondrites (average Th/Sm = 0.25). However, the high-Ti sources have a wider range of Th/Sm ratios (0.03–0.12). Melting processes are unlikely to have fractionated Th from Sm in the source regions; therefore, the measured Th/Sm ratios are believed to be characteristic of the source regions from which the glasses were

derived. The Th/Sm ratios of the sources must have been established during the crystallization of LMO cumulates, with compositional variations a function of phase heterogeneity in the cumulate source regions (e.g. Shearer and Papike, 1993, 1999).

Based on the lunar magma ocean crystallization scenario presented by Snyder et al. (1992), the data from this study have been used to estimate the bulk Th, Sm, U, and K composition of the lunar mantle. From these calculations, we estimate that the lunar mantle contains 0.15 ppm Th, 0.54 ppm Sm, 0.039 ppm U, and 212 ppm K. These values are greater than earlier estimates (see Table 6) and are two times higher than estimates for the earth (e.g., McDonough and Sun, 1995). At a minimum, our calculated compositions for the pyroclastic source regions indicate that the lunar mantle will have at least 0.055 ppm Th, which is still higher than previous estimates. The Th enrichment problem can be solved if the pyroclastic glasses were produced by very small degrees of partial melting (i.e., $\leq 5\%$); however, these small degrees of melting may be too low for basaltic magmas with high Mg' (personal communication, G.J. Taylor, 2006). We concede that our model is simplistic and as a result, our estimates are not necessarily correct. However, because Th can serve as a proxy for other refractory elements, the results from this study may have important implications for the bulk refractory element content of the Moon. At the very least, the data presented in the study can be used to place constraints on future geochemical and geophysical models.

Acknowledgments

Funding for this study was provided by a grant from the Institute of Geophysics and Planetary Physics (IGPP) (Dr. Charles Shearer and Dr. David Vaniman P.I.s) and by a student fellowship from the New Mexico Space Grant Consortium (J.J. Hagerty). We thank Dr. Scott Hughes, Dr. G. Jeffrey Taylor, Dr. Clive Neal, and an anonymous reviewer for their insightful comments.

Associate editor: Clive R. Neal

Appendix A

See Tables A1 and A2.

Table A1

Calculated compositions of pyroclastic glass source regions, assuming 5% partial melting

Apollo site	Sample number	Glass color	Th (ppm)	Sm (ppm)	Th/Sm	U (ppm)	K (wt.%)	A ($\mu\text{W}/\text{m}^3$)
A11	10030g2	Orange	0.026	0.45	0.058	0.007	0.164	0.039
A11	10030g3	Orange	0.026	0.51	0.052	0.007	0.164	0.041
A11	10030g4	Orange	0.030	0.47	0.065	0.008	0.166	0.041
A11	10030g7	Orange	0.024	0.50	0.048	0.006	0.164	0.040
A11	10030g8	Orange	0.028	0.49	0.057	0.008	0.165	0.041
A11	10030g12	Orange	0.021	0.41	0.050	0.006	0.162	0.037
A11	10030g13	Orange	0.031	0.48	0.064	0.008	0.166	0.041
A11	10030g14	Orange	0.030	0.46	0.066	0.008	0.166	0.040
A11	10031g1	Orange	0.022	0.43	0.051	0.006	0.163	0.037
A11	10031g2	Orange	0.022	0.43	0.051	0.006	0.163	0.038
A11	10031g3	Orange	0.026	0.38	0.069	0.007	0.164	0.037
A11	10031g4	Orange	0.027	0.45	0.060	0.007	0.165	0.039
A11	10031g9	Orange	0.028	0.44	0.062	0.007	0.165	0.039
A11	10031g11	Orange	0.023	0.45	0.050	0.006	0.163	0.038
A11	10031g13	Orange	0.021	0.44	0.049	0.006	0.163	0.038
A11	10031g17	Orange	0.021	0.40	0.054	0.006	0.162	0.036
A11	10031g18	Orange	0.030	0.48	0.063	0.008	0.166	0.041
A11	10031g19	Orange	0.025	0.50	0.051	0.007	0.164	0.041
A11	10031g22	Orange	0.029	0.46	0.064	0.008	0.166	0.040
Average			0.026	0.45	0.057	0.007	0.164	0.039
1σ			0.003	0.035	0.007	0.001	0.001	0.002
A12	12033g1	Red	0.053	0.65	0.082	0.014	0.175	0.052
A12	12033g3	Red	0.061	0.67	0.092	0.017	0.178	0.054
A12	12033g4	Red	0.059	0.63	0.093	0.016	0.177	0.053
A12	12033g5	Red	0.067	0.65	0.10	0.018	0.180	0.055
A12	12033g6	Red	0.052	0.58	0.089	0.014	0.175	0.049
A12	12033g11	Red	0.056	0.62	0.091	0.015	0.176	0.051
A12	12033g8	Red	0.054	0.62	0.087	0.015	0.175	0.051
A12	12033g13	Red	0.056	0.61	0.092	0.015	0.176	0.051
A12	12033g14	Red	0.058	0.62	0.093	0.016	0.177	0.052
Average			0.057	0.63	0.091	0.015	0.177	0.052
1σ			0.005	0.026	0.005	0.001	0.002	0.002
A14	14048g75	Green	0.034	0.16	0.21	0.009	0.167	0.031
A14	14048g71	Green	0.050	0.20	0.25	0.014	0.174	0.036
A14	14048g52	Green	0.022	0.11	0.21	0.006	0.163	0.026
A14	14048g32	Green	0.062	0.26	0.24	0.017	0.179	0.040
A14	14049g17	Green	0.029	0.11	0.26	0.008	0.166	0.028
A14	14049g18	Green	0.057	0.24	0.24	0.015	0.177	0.038
A14	14049g03	Green	0.068	0.27	0.25	0.018	0.181	0.042
A14	14049g11	Green	0.068	0.27	0.25	0.018	0.181	0.042
Average			0.049	0.20	0.24	0.013	0.173	0.035
1σ			0.018	0.069	0.018	0.005	0.007	0.006
A14	14041g34	Red	0.19	0.80	0.24	0.052	0.231	0.088
A14	14041g34b	Red	0.22	0.79	0.28	0.059	0.240	0.092
A14	14301g3	Red	0.28	1.1	0.26	0.076	0.265	0.116
A14	14301g5	Black	0.16	0.74	0.22	0.043	0.217	0.078
A14	14048g30	Red	0.17	0.69	0.24	0.046	0.221	0.078
Average			0.20	0.82	0.25	0.055	0.235	0.090
1σ			0.048	0.144	0.023	0.013	0.019	0.015
A15	15041g30	Yellow	0.066	0.40	0.17	0.018	0.180	0.046
A15	15318g1	Yellow	0.058	0.35	0.17	0.016	0.177	0.043
A15	15030g5	Yellow	0.025	0.29	0.084	0.007	0.164	0.033
A15	15030g6	Yellow	0.025	0.29	0.086	0.007	0.164	0.033
A15	15049g23	Yellow	0.074	0.36	0.20	0.020	0.183	0.046
Average			0.050	0.34	0.14	0.013	0.174	0.040
1σ			0.023	0.046	0.054	0.006	0.009	0.007

(continued on next page)

Table A1 (continued)

Apollo site	Sample number	Glass color	Th (ppm)	Sm (ppm)	Th/Sm	U (ppm)	K (wt.%)	A ($\mu\text{W}/\text{m}^3$)
A15	15426,18g3	Red	0.057	0.63	0.090	0.015	0.177	0.052
A15	15426,18g2	Red	0.058	0.69	0.084	0.016	0.177	0.054
A15	15426,18g1	Red	0.063	0.69	0.091	0.017	0.179	0.056
A15	15318g30	Red	0.069	0.68	0.10	0.019	0.181	0.056
Average 1σ			0.06	0.68	0.09	0.017	0.178	0.055
			0.006	0.028	0.007	0.001	0.002	0.002
A15	15318g5	Green A	0.014	0.058	0.24	0.004	0.160	0.023
A15	15318g6	Green A	0.015	0.066	0.23	0.004	0.160	0.023
A15	15427g1	Green A	0.024	0.072	0.34	0.007	0.164	0.026
A15	15427g2	Green A	0.024	0.072	0.34	0.007	0.164	0.026
A15	15041g33	Green A	0.010	0.045	0.23	0.003	0.158	0.022
A15	15426,18g28	Green A	0.010	0.050	0.20	0.003	0.158	0.022
A15	15426,18g27	Green A	0.010	0.043	0.23	0.003	0.158	0.022
A15	15426,18g21	Green A	0.010	0.046	0.22	0.003	0.158	0.022
A15	15426,18g20	Green A	0.011	0.046	0.23	0.003	0.158	0.022
A15	15318g40	Green B	0.017	0.075	0.23	0.005	0.161	0.024
A15	15427g1	Green B	0.018	0.077	0.24	0.005	0.161	0.025
A15	15427g2	Green B	0.018	0.075	0.24	0.005	0.161	0.024
A15	15318g33	Green D	0.016	0.077	0.21	0.004	0.160	0.024
A15	15318g29	Green D	0.015	0.065	0.22	0.004	0.160	0.023
A15	15318g31	Green D	0.016	0.069	0.24	0.004	0.161	0.024
A15	15427g1	Green D	0.012	0.053	0.23	0.003	0.159	0.022
A15	15427g2	Green D	0.016	0.064	0.25	0.004	0.160	0.024
A15	15426,18g23	Green D	0.010	0.048	0.22	0.003	0.158	0.022
A15	15426,18g11	Green D	0.015	0.054	0.28	0.004	0.160	0.023
A15	15426,18g22	Green D	0.014	0.059	0.24	0.004	0.160	0.023
A15	15426,18g17	Green D	0.015	0.069	0.22	0.004	0.160	0.024
A15	15426,18g26	Green D	0.011	0.046	0.24	0.003	0.158	0.022
A15	15318g7	Green E	0.017	0.070	0.25	0.005	0.161	0.024
A15	15318g32	Green E	0.024	0.095	0.25	0.006	0.163	0.026
A15	15426,18g25	Green E	0.016	0.060	0.27	0.004	0.160	0.023
Average 1σ			0.02	0.06	0.24	0.004	0.160	0.023
			0.004	0.013	0.033	0.001	0.002	0.001
A17	79135g19	Yellow	0.055	0.34	0.16	0.015	0.176	0.042
A17	79135g20	Green	0.037	0.13	0.29	0.010	0.169	0.030
A17	79135g21	Green	0.031	0.10	0.33	0.008	0.166	0.028
A17	79135g27	Green	0.021	0.10	0.21	0.006	0.162	0.026
A17	79135g68	Green	0.021	0.089	0.24	0.006	0.162	0.026
Average for A17 green glasses 1σ			0.027	0.10	0.26	0.007	0.165	0.027
			0.008	0.016	0.054	0.002	0.003	0.002
A17	79315g1	Orange	0.027	0.40	0.068	0.007	0.165	0.038
A17	79315g2	Orange	0.026	0.41	0.062	0.007	0.164	0.038
A17	79315g3	Orange	0.028	0.42	0.067	0.008	0.165	0.038
A17	79315g4	Orange	0.028	0.40	0.070	0.008	0.165	0.038
A17	79315g5	Orange	0.028	0.42	0.067	0.008	0.165	0.038
A17	79315g6	Orange	0.023	0.39	0.060	0.006	0.163	0.036
Average 1σ			0.03	0.41	0.07	0.007	0.165	0.038
			0.002	0.011	0.004	0.001	0.001	0.001

Table A2
Calculated compositions of pyroclastic glass source regions, assuming 15% partial melting

Apollo site	Sample number	Glass color	Th (ppm)	Sm (ppm)	Th/Sm	U (ppm)	K (wt.%)	A ($\mu\text{W}/\text{m}^3$)
A11	10030g2	Orange	0.08	1.3	0.058	0.021	0.018	0.062
A11	10030g3	Orange	0.08	1.5	0.052	0.021	0.019	0.068
A11	10030g4	Orange	0.09	1.4	0.065	0.024	0.019	0.066
A11	10030g7	Orange	0.07	1.5	0.048	0.019	0.018	0.066
A11	10030g8	Orange	0.08	1.5	0.057	0.023	0.019	0.067

Table A2 (continued)

Apollo site	Sample number	Glass color	Th (ppm)	Sm (ppm)	Th/Sm	U (ppm)	K (wt.%)	A ($\mu\text{W/m}^2$)
A11	10030g12	Orange	0.06	1.2	0.050	0.017	0.018	0.055
A11	10030g13	Orange	0.09	1.4	0.064	0.025	0.019	0.067
A11	10030g14	Orange	0.09	1.4	0.066	0.025	0.019	0.065
A11	10031g1	Orange	0.07	1.3	0.051	0.018	0.018	0.058
A11	10031g2	Orange	0.07	1.3	0.051	0.018	0.018	0.058
A11	10031g3	Orange	0.08	1.1	0.069	0.021	0.019	0.055
A11	10031g4	Orange	0.08	1.4	0.060	0.022	0.019	0.063
A11	10031g9	Orange	0.08	1.3	0.062	0.022	0.019	0.062
A11	10031g11	Orange	0.07	1.4	0.050	0.018	0.018	0.061
A11	10031g13	Orange	0.06	1.3	0.049	0.017	0.018	0.058
A11	10031g17	Orange	0.06	1.2	0.054	0.017	0.018	0.054
A11	10031g18	Orange	0.09	1.4	0.063	0.025	0.019	0.068
A11	10031g19	Orange	0.08	1.5	0.051	0.021	0.018	0.067
A11	10031g22	Orange	0.09	1.4	0.064	0.024	0.019	0.064
Average			0.078	1.362	0.057	0.021	0.018	0.062
1σ			0.010	0.105	0.007	0.003	0.000	0.005
A12	12033g1	Red	0.16	1.9	0.082	0.043	0.022	0.097
A12	12033g3	Red	0.18	2.0	0.092	0.050	0.023	0.103
A12	12033g4	Red	0.18	1.9	0.093	0.048	0.022	0.098
A12	12033g5	Red	0.20	2.0	0.10	0.054	0.023	0.104
A12	12033g6	Red	0.16	1.7	0.089	0.042	0.022	0.089
A12	12033g11	Red	0.17	1.8	0.091	0.045	0.022	0.095
A12	12033g8	Red	0.16	1.9	0.087	0.044	0.022	0.094
A12	12033g13	Red	0.17	1.8	0.092	0.045	0.022	0.094
A12	12033g14	Red	0.17	1.9	0.093	0.047	0.022	0.096
Average			0.172	1.883	0.091	0.046	0.022	0.097
1σ			0.014	0.077	0.005	0.004	0.001	0.005
A14	14048g75	Green	0.10	0.5	0.21	0.027	0.019	0.036
A14	14048g71	Green	0.15	0.6	0.25	0.041	0.021	0.049
A14	14048g52	Green	0.07	0.3	0.21	0.018	0.018	0.025
A14	14048g32	Green	0.19	0.8	0.24	0.051	0.023	0.061
A14	14049g17	Green	0.09	0.3	0.26	0.023	0.019	0.029
A14	14049g18	Green	0.17	0.7	0.24	0.046	0.022	0.056
A14	14049g03	Green	0.20	0.8	0.25	0.055	0.023	0.066
A14	14049g11	Green	0.20	0.8	0.25	0.055	0.024	0.066
Average			0.15	0.61	0.24	0.040	0.021	0.048
1σ			0.055	0.206	0.018	0.015	0.002	0.017
A14	14041g34	Red	0.58	2.4	0.24	0.16	0.038	0.187
A14	14041g34b	Red	0.65	2.4	0.28	0.18	0.041	0.197
A14	14301g3	Red	0.84	3.2	0.26	0.23	0.049	0.260
A14	14301g5	Black	0.48	2.2	0.22	0.13	0.034	0.163
A14	14048g30	Red	0.51	2.1	0.24	0.14	0.036	0.162
Average			0.61	2.45	0.25	0.17	0.04	0.194
1σ			0.145	0.433	0.023	0.039	0.006	0.040
A15	15041g30	Yellow	0.20	1.2	0.17	0.054	0.023	0.078
A15	15318g1	Yellow	0.17	1.0	0.17	0.047	0.022	0.069
A15	15030g5	Yellow	0.07	0.9	0.084	0.020	0.018	0.045
A15	15030g6	Yellow	0.07	0.9	0.086	0.020	0.018	0.045
A15	15049g23	Yellow	0.22	1.1	0.20	0.060	0.024	0.078
Average			0.15	1.01	0.14	0.040	0.021	0.063
1σ			0.070	0.137	0.054	0.019	0.003	0.017
A15	15426,18g3	Red	0.17	1.9	0.090	0.046	0.022	0.097
A15	15426,18g2	Red	0.17	2.1	0.084	0.047	0.022	0.104
A15	15426,18g1	Red	0.19	2.1	0.091	0.051	0.023	0.107
A15	15318g30	Red	0.21	2.1	0.10	0.056	0.024	0.109
Average			0.185	2.028	0.091	0.050	0.023	0.104
1σ			0.017	0.084	0.007	0.004	0.001	0.005

(continued on next page)

Table A2 (continued)

Apollo site	Sample number	Glass color	Th (ppm)	Sm (ppm)	Th/Sm	U (ppm)	K (wt.%)	A ($\mu\text{W}/\text{m}^2$)
A15	15318g5	Green A	0.04	0.18	0.24	0.011	0.017	0.015
A15	15318g6	Green A	0.04	0.20	0.23	0.012	0.017	0.016
A15	15427g1	Green A	0.07	0.22	0.34	0.020	0.018	0.022
A15	15427g2	Green A	0.07	0.22	0.34	0.020	0.018	0.022
A15	15041g33	Green A	0.03	0.14	0.23	0.008	0.017	0.012
A15	15426,18g28	Green A	0.03	0.15	0.20	0.008	0.017	0.012
A15	15426,18g27	Green A	0.03	0.13	0.23	0.008	0.017	0.012
A15	15426,18g21	Green A	0.03	0.14	0.22	0.008	0.017	0.012
A15	15426,18g20	Green A	0.03	0.14	0.23	0.009	0.017	0.012
A15	15318g40	Green B	0.05	0.22	0.23	0.014	0.017	0.018
A15	15427g1	Green B	0.06	0.23	0.24	0.015	0.018	0.019
A15	15427g2	Green B	0.06	0.23	0.24	0.015	0.018	0.019
A15	15318g33	Green D	0.05	0.23	0.21	0.013	0.017	0.018
A15	15318g29	Green D	0.04	0.20	0.22	0.012	0.017	0.016
A15	15318g31	Green D	0.05	0.21	0.24	0.013	0.017	0.018
A15	15427g1	Green D	0.04	0.16	0.23	0.010	0.017	0.014
A15	15427g2	Green D	0.05	0.19	0.25	0.013	0.017	0.017
A15	15426,18g23	Green D	0.03	0.14	0.22	0.008	0.017	0.012
A15	15426,18g11	Green D	0.04	0.16	0.28	0.012	0.017	0.015
A15	15426,18g22	Green D	0.04	0.18	0.24	0.011	0.017	0.015
A15	15426,18g17	Green D	0.04	0.21	0.22	0.012	0.017	0.017
A15	15426,18g26	Green D	0.03	0.14	0.24	0.009	0.017	0.012
A15	15318g7	Green E	0.05	0.21	0.25	0.014	0.017	0.018
A15	15318g32	Green E	0.07	0.28	0.25	0.019	0.018	0.024
A15	15426,18g25	Green E	0.05	0.18	0.27	0.013	0.017	0.016
Average			0.05	0.19	0.24	0.012	0.017	0.016
1σ			0.013	0.039	0.033	0.003	0.001	0.004
A17	79135g19	Yellow	0.16	1.0	0.16	0.045	0.022	0.066
A17	79135g20	Green	0.11	0.4	0.29	0.030	0.020	0.034
A17	79135g21	Green	0.09	0.3	0.33	0.025	0.019	0.028
A17	79135g27	Green	0.06	0.3	0.21	0.017	0.018	0.023
A17	79135g68	Green	0.06	0.3	0.24	0.017	0.018	0.022
Average for A17 green glasses			0.08	0.31	0.26	0.022	0.019	0.027
1σ			0.023	0.049	0.054	0.006	0.001	0.005
A17	79315g1	Orange	0.08	1.2	0.068	0.022	0.019	0.057
A17	79315g2	Orange	0.08	1.2	0.062	0.021	0.018	0.058
A17	79315g3	Orange	0.08	1.2	0.067	0.023	0.019	0.059
A17	79315g4	Orange	0.09	1.2	0.070	0.023	0.019	0.058
A17	79315g5	Orange	0.08	1.3	0.067	0.023	0.019	0.060
A17	79315g6	Orange	0.07	1.2	0.060	0.019	0.018	0.054
Average			0.080	1.220	0.066	0.022	0.019	0.058
1σ			0.006	0.033	0.004	0.002	0.000	0.002

References

- Anders, E., 1977. Chemical compositions of the Moon, Earth, and eucrite parent body. *Philos. Trans. Roy. Soc. London A* **285**, 23–40.
- Anders, E., Grevesse, N., 1989. Abundance of the elements; meteoritic and solar. *Geochim. Cosmochim. Acta* **53**, 197–214.
- Beattie, P., 1994. Systematics and energetics of trace-element partitioning between olivine and silicate melts: implications for the nature of mineral–melt partitioning. *Chem. Geol.* **117**, 57–71.
- Beck, A.R., Morgan, Z.T., Liang, Y., Hess, P.C., 2006. Dunite channels as viable pathways for mare basalt transport in the deep lunar mantle. *Geophys. Res. Lett.*, 33. doi:10.1029/2005GL024008.
- Binder A.B., 1982. The mare basalt magma source region and mare basalt magma genesis. In *Proc. 13th Lunar Planet. Sci. Conf.* A37–A53.
- Buntebarth, G., 1984. *Geothermics*. Springer Verlag, New York.
- Chen, H.-K., Lindsley, D. H., 1983. Apollo 14 very-low titanium glasses: melting experiments in iron–platinum alloy capsules. In *Proc. 14th Lunar Planet. Sci. Conf.* B335–B342.
- Chen, H.-K., Delano J.W., Lindsley, D.H., 1982. Chemistry and phase relations of VLT volcanic glasses from Apollo 14 and Apollo 17. In *Proc. 13th Lunar Planet. Sci. Conf.* A171–A181.
- Delano J.W., 1979. Apollo 15 green glass: chemistry and possible origin. *Proc. 10th Lunar Planet. Sci. Conf.* 275–300.
- Delano J.W., 1980. Chemistry and liquidus phase relations of Apollo 15 red glass: implications for the deep lunar interior. In *Proc. 11th Lunar Planet. Sci. Conf.* 251–288.
- Delano J.W., 1986. Pristine lunar glasses: criteria, data, and implications. In *Proc. 16th Lunar Planet. Sci. Conf.* 201–213.
- DePaolo, D.J., 1981. Trace-element and isotopic effects of combined wallrock assimilation and fractional crystallization. *Earth Planet. Sci. Lett.* **53**, 189–202.

- Duncan A.R., Erlank A.J., Sher M.K., Abraham Y.C., Willis J.P., Ahrens L.H., 1976. Some trace-element constraints on lunar basalt genesis. *Proc. 7th Lunar Sci. Conf.* 1659–1671.
- Elkins-Tanton L.T., Grove T.L., 2001. Lunar mantle composition and thermal history: constraints from phase equilibria studies. *Lunar Planet. Sci. XXXII*. Lunar Planet. Inst., Houston. #1791 (abstr.).
- Elkins-Tanton, L.T., Fernandes, V.A., Delano, J.W., Grove, T.L., 2000. Origin of lunar ultramafic green glasses: constraints from phase equilibrium studies. *Geochim. Cosmochim. Acta* **64**, 2339–2350.
- Elkins-Tanton, L.T., Chatterjee, N., Grove, T.L., 2003. Experimental and petrological constraints on lunar differentiation from the Apollo 15 green picritic glasses. *Meteor. Planet. Sci.* **38**, 515–527.
- Green, D.H., Ringwood, A.E., Ware, N.G., Hibberson, W.O., Major, A., Kiss, E., 1971. Experimental petrology and petrogenesis of Apollo 12 basalts. In *Proc. 2nd Lunar Sci. Conf.* 601–615.
- Green, D.H., Ringwood, A.E., Hibberson, W.O., Ware N.G., 1975. Experimental petrology of Apollo 17 mare basalts. *Proc. 6th Lunar Sci. Conf.* 871–893.
- Haskin L.A., 1997. The distribution of Th on the Moon's surface. *Lunar Planet. Sci. Conf. XXXIII*. Lunar Planet. Inst., Houston. 519–520 (abstr.).
- Haskin, L.A., Gillis, J.J., Korotev, R.L., Jolliff, B.L., 2000. The materials of the lunar Procellarum KREEP Terrane: A synthesis of data from geomorphologic mapping, remote sensing and sample analysis. *J. Geophys. Res.-Planets* **108**, 20403–20415.
- Hess, P.C., 1989. *Origins of Igneous Rocks*. Harvard University Press, Cambridge.
- Hess, P.C., 2000. On the source region for mare picrite glasses. *J. Geophys. Res.-Planets* **105**, 4347–4360.
- Hess, P.C., Parmentier, E.M., 1995. A model for the thermal and chemical evolution of the Moon's interior: implications for the onset of mare volcanism. *Earth Planet. Sci. Lett.* **134**, 501–514.
- Hess, P.C., Rutherford, M.J., Guillemette, R.N., Ryerson, F.J., Tuchfeld, H.A., 1975. Residual products of fractional crystallization of lunar magmas: an experimental study. In *Proc. 6th Lunar Sci. Conf.* 895–910.
- Hiesinger, H., Head III, J.W., Wolf, U., Jaumann, R., Neukum, G., 2003. Ages and stratigraphy of mare basalts in Oceanus Procellarum, Mare Nubium, Mare Cognitum, and Mare Insularum. *J. Geophys. Res.-Planets* **108**. doi:10.1029/2002JE001985.
- Hodges, F.N., Kushiro, I., 1974. Apollo 17 petrology and experimental determination of differentiation sequences in model moon compositions. In *Proc. 5th Lunar Sci. Conf.* 505–520.
- Horai, K., Simmons, G., Kanamori, H., Wones, D., 1970. Thermal diffusivity, conductivity, and thermal inertia of Apollo 11 lunar material. In *Proc. Apollo 11 Lunar Sci. Conf.* 2243–2249.
- Hsui, A.T., 1979. The bounds of heat production rate within the Moon. In *Proc. 10th Lunar Planet. Sci. Conf.* 2393–2402.
- Hughes, S.S., Delano, J.W., Schmitt, R.A., 1988. Apollo 15 yellow-brown volcanic glass: chemistry and petrogenetic relations to green volcanic glass and olivine-normative mare basalts. *Geochim. Cosmochim. Acta* **52**, 2379–2391.
- Hughes, S.S., Delano, J.W., Schmitt, R.A., 1990. Chemistries of individual mare volcanic glasses—Evidence for distinct regions of hybridized mantle and a KREEP component in Apollo 14 magmatic sources. In *Proc. 20th Lunar Planet. Sci. Conf.* 127–138.
- Jolliff, B.L., Gillis, J.J., 2002. Lunar crustal and bulk composition: Th and Al mass balance. *Moon Beyond 2002: Next Steps Lunar Sci. Exp.* Lunar Planet. Inst., Houston. # 3056 (abstr.).
- Jolliff, B.L., Gillis, J.J., Haskin, L.A., Korotev, R.L., Wieczorek, M.A., 2000. Major crustal terranes: surface expressions and crust–mantle origins. *J. Geophys. Res.-Planets* **105**, 4197–4216.
- Kesson, S.E., 1975. Mare basalts: melting experiments and petrogenetic interpretations. In *Proc. 6th Lunar Sci. Conf.* 921–944.
- Kesson, S.E., Lindsley, D.H., 1974. Mare basalt petrogenesis—A review of experimental studies. *Rev. Geophys. Space Phys.* **12**, 361–374.
- Korotev, R.L., 1998. Concentrations of radioactive elements in lunar materials. *J. Geophys. Res.-Planets* **103**, 1691–1701.
- Landwehr, D., Blundy, J., Chamorro-Perez, E.M., Hill, E., Wood, B., 2001. U-series disequilibria generated by partial melting of spinel lherzolite. *Earth Planet. Sci. Lett.* **188**, 329–348.
- Lawrence, D.J. et al., 1998. Global element maps of the Moon: the lunar prospector gamma-ray spectrometer. *Science* **281**, 1484–1489.
- Lawrence, D.J. et al., 2000. Thorium abundances on the lunar surface. *J. Geophys. Res.-Planets* **105**, 20307–20331.
- Lawrence, D.J. et al., 2003. Small-area thorium features on the lunar surface. *J. Geophys. Res.-Planets* **108**, 2050.
- Longhi, J.W., 1987. On the connection between mare basalts and volcanic volcanic glasses. *J. Geophys. Res.* **92**, 349–360.
- Longhi, J.W., 1992. Experimental petrology and petrogenesis of mare volcanics. *Geochim. Cosmochim. Acta* **56**, 2235–2251.
- McDonough, W.F., Sun, S.-S., 1995. The composition of the earth. *Chem. Geol.* **120**, 223–253.
- McKay, G.A., Wagstaff, J., Yang, S.-R., 1986. Clinopyroxene REE distribution coefficients for shergottites: the REE content of the Shergotty melt. *Geochim. Cosmochim. Acta* **50**, 927–937.
- McKenzie, D., O'Nions, R.K., 1991. Partial melt distributions from inversion of rare earth element concentrations. *J. Petrol.* **32**, 1021–1091.
- Neal, C.R., Taylor, L.A., 1992. Petrogenesis of mare basalts: a record of lunar volcanism. *Geochim. Cosmochim. Acta* **56**, 2177–2211.
- O'Neill, H.St.C., 1991. The origin of the Moon and the early history of the Earth—A chemical model. Part 1: the Moon. *Geochim. Cosmochim. Acta* **55**, 1135–1157.
- Papike, J.J., Hodges, F.N., Bence, A.E., Cameron, M., Rhodes, J.M., 1976. Mare basalts: crystal chemistry, mineralogy, and petrology. *Rev. Geophys. Space Phys.* **14**, 475–540.
- Papike, J.J., Ryder, G., Shearer, C.K., 1998. Lunar samples. *Rev. Mineral.* **36**, 5–234.
- Phinney, W.C., Morrison, D.A., 1990. Partition coefficients for calcic plagioclase: implications for Archean anorthosites. *Geochim. Cosmochim. Acta* **54**, 1639–1654.
- Rhodes, J.M., Hubbard, N.J., 1973. Chemistry, classification, and petrogenesis of Apollo 15 mare basalts. In *Proc. 4th Lunar Sci. Conf.* 1127–1148.
- Ringwood, A.E., Essene, E., 1970. Petrogenesis of lunar basalts, internal constitution and origin of the Moon. In *Proc. Apollo 11 Lunar Sci. Conf.* 769–799.
- Ringwood A.E., Kesson, S.E., 1976. A dynamic model for mare basalt petrogenesis. *Proc. 7th Lunar Sci. Conf.* 1697–1722.
- Rybach, L., 1988. Determination of heat production rate. In: Haenel, R., Rybach, L., Stegna, L. (Eds.), *Handbook of Terrestrial Heat-Flow Density Determination*. Kluwer Academic Publishers, Boston, pp. 125–142.
- Ryder, G., 1991. Lunar ferroan anorthosites and mare basalt sources: the mixed connection. *Geophys. Res. Lett.* **18**, 2065–2068.
- Schubert, G., Turcotte, D.L., Olson, P., 2001. *Mantle Convection in the Earth and Planets*. Cambridge University Press, New York.
- Schwandt, C.S., McKay, G.A., 1998. Rare earth element partition coefficients from enstatite/melt synthesis experiments. *Geochim. Cosmochim. Acta* **62**, 2845–2848.
- Shearer, C.K., Papike, J.J., 1993. Basaltic magmatism on the Moon: A perspective from volcanic glass beads. *Geochim. Cosmochim. Acta* **57**, 4785–4812.
- Shearer, C.K., Papike, J.J., 1999. Magmatic evolution of the Moon. *Am. Miner.* **84**, 1469–1494.
- Shearer, C.K., Papike, J.J., Galbreath, K.C., Yuimoto, H., Shimizu, N., 1989. SIMS analyses of glasses, trace-element characteristics of lunar picritic glasses and implications for the mantle sources of lunar picritic magmas. *LPI Technical Report* **90-02**, 58–59.
- Shearer, C.K., Papike, J.J., Simon, S.B., Shimizu, N., Yurimoto, H., Sueno, S., 1990. Ion microprobe studies of REE and other trace-elements in Apollo 14 “volcanic” glass beads and comparisons to Apollo 14 mare basalts. *Geochim. Cosmochim. Acta* **54**, 851–867.
- Shearer, C.K., Papike, J.J., Galbreath, K.C., Shimizu, N., 1991. Exploring the lunar mantle with secondary ion mass spectrometry: A comparison

- of lunar picritic glass beads from the Apollo 14 and Apollo 17 sites. *Earth Planet. Sci. Lett.* **102**, 124–147.
- Shearer, C.K., Neal, C., Papike, J.J., 2002. The behavior of Th and Sm in lunar basalts. Establishing a better understanding of remotely sensed lunar data for use in deciphering the igneous history of the Moon. *Lunar Planet. Sci. XXXIII*. Lunar Planet. Inst., Houston. #1621 (abstr.).
- Smith, J.V., Anderson, A.T., Newton, R.C., Olsen, E.J., Wyllie, P.J., Crewe, A.V., Isaacson, M.S., Johnson, D., 1970. Petrologic history of the Moon inferred from petrography, mineralogy and petrogenesis of Apollo 11 rocks. In *Proc. Apollo 11 Lunar Sci. Conf.* 897–925.
- Snyder, G.A., Taylor, L.A., Neal, C.R., 1992. A chemical model for generating the sources of mare basalts: combined equilibrium and fractional crystallization of the lunar magmasphere. *Geochim. Cosmochim. Acta* **56**, 3809–3823.
- Spera, F.J., 1992. Lunar magma transport phenomena. *Geochim. Cosmochim. Acta* **56**, 2253–2266.
- Stolper, E., Walker, D., Longhi, J., Hays, J.F., 1974. Compositional variation in lunar ultramafic glasses. In *Proc. 5th Lunar Sci. Conf.* 749–751.
- Taylor S. R., Jäkes P., 1974. The geochemical evolution of the Moon. *Proc. 5th Lunar Sci. Conf.* 1287–1305.
- Taylor, S.R., 1994. *Solar System Evolution: A New Perspective*. Cambridge University Press, New York.
- Taylor, G.J., Hawke, B.R., Spudis, P.D., 2002. Bulk composition of the Moon: importance, uncertainties, and what we need to know. *Moon Beyond 2002: Next Steps Lunar Sci. Exp.* Lunar Planet.
- Unruh, D.M., Stille, P., Patchett, P.J., Tatsumoto, M., 1984. Lu–Hf and Sm–Nd evolution in lunar mare basalts. In *Proc. 14th Lunar Planet. Sci. Conf.* B17–B25.
- Villemand, B., Jaffrezic, H., Joron, J.-L., Treuil, M., 1981. Distribution coefficients of major and trace elements; fractional crystallization in the alkali basalt series of Chaîne des Puys (Massif Central, France). *Geochim. Cosmochim. Acta* **45**, 1997–2016.
- Wänke, H., Palme, H., Baddehausen, H., Kruse, H., Spettel, B., 1977. Element correlations and the bulk composition of the Moon. *Philos. Trans. Roy. Soc. London* **A285**, 41–48.
- Warren, P.H., 2005. “New” lunar meteorites: implications for composition of the global lunar surface, lunar crust, and the bulk Moon. *Meteor. Planet. Sci.* **40**, 477–506.
- Warren, P.H., Wasson, J.T., 1979. The origin of KREEP. *Rev. Geophys. Space Phys.* **17**, 73–88.
- Warren, P.H., Rasmussen, K.L., 1987. Megaregolith insulation, internal temperatures, and bulk uranium content of the Moon. *J. Geophys. Res.* **92**, 3453–3465.
- Warren, P.H., Humphrys, T.L., 2003. Bulk composition of the Moon as constrained by thorium data: comparison of lunar prospector versus Apollo GRS results. *Lunar Planet. Sci. XXXIV*. Lunar Planet. Inst., Houston. #2034 (abstr.).
- Weill, D.F., McKay, G.A., 1975. The partitioning of Mg, Fe, Sr, Ce, Sm, Eu, and Yb in lunar igneous systems and a possible origin of KREEP by equilibrium partial melting. In *Proc. 6th Lunar Sci. Conf.* 1143–1158.
- Wieczorek, M.A., Phillips, R.J., 2000. The “Procellarum KREEP Terrane”: implications for mare volcanism and lunar evolution. *J. Geophys. Res.-Planets* **105**, 20417–20430.
- Wilson, L., Head III, J.W., 2003. Deep generation of magmatic gas on the Moon and implications for volcanic eruptions. *Geophys. Res. Lett.* **30**, 1605.
- Wood, J.A., Dickey, J.S., Marvin, U.B., Powell, B.N., 1970. Lunar anorthosites and a geophysical model of the Moon. In *Proc. Apollo 11 Lunar Sci. Conf.* 965–988.
- Zack, T., Brumm, R., 1998. Ilmenite/liquid partition coefficients of 26 trace elements determined through ilmenite/clinopyroxene partitioning in garnet pyroxene. In *7th International Kimberlite Conf.* 986–988.